Master's thesis

NTNU
Norwegian University of Science and Technology
Faculty of Information Technology and Electrical Engineering
Department of Electric Power Engineering

Jakob Strompdal

Dynamic Thermal Rating of Overhead Power Lines

Contribution from Evaporative Cooling

Master's thesis in Energy and Environmental Engineering
Supervisor: Erling Ildstad
June 2021

NTNU
Norwegian University of Science and Technology

Jakob Strompdal

Dynamic Thermal Rating of Overhead Power Lines

Contribution from Evaporative Cooling

Master's thesis in Energy and Environmental Engineering
Supervisor: Erling Ildstad
June 2021

Norwegian University of Science and Technology
Faculty of Information Technology and Electrical Engineering
Department of Electric Power Engineering

NTNU
Norwegian University of
Science and Technology

Abstract

The demand for electrical energy is increasing all over the world. The complexity and variations in both production and consumption are also increasing due to more renewable energy sources. Because of this development, it is essential to utilize the capacity of existing power lines better. Earlier, static ratings have been the most common way to operate power lines. However, with new technology, it is easier to monitor and apply dynamic ratings based on real-time weather parameters. Dynamic rating is a potential solution to the development in the energy sector and the new challenges.

This thesis consists of a literature review regarding already existing technology for measuring Dynamic ratings. The model recommended by CIGRE for calculating dynamic ratings have been investigated and has been further developed by implementing terms for evaporative cooling and impingement cooling based on other articles and standards. The main focus was to look into the correlation between a change in different weather parameters and evaporative cooling. The reason for this was to get a better understanding of the potential amount of cooling from evaporation and in which weather conditions and climate it can be reasonable to implement evaporative cooling in the model used to calculate dynamic ratings.

It was expected that evaporative cooling was highly dependent on the precipitation rate. In addition, the investigation of models recommended by CIGRE and IEEE showed that ambient temperature, conductor surface temperature, wind speed and air pressure also affect evaporative cooling. Results obtained from simulation showed that for a precipitation rate equal to 1, increasing wind speed from 1 to 20 m/s lead to an increase in evaporative cooling from 75 W/m to 1 368 W/m. Increased conductor surface temperature from 10 to 80 degrees lead to an increase in evaporative cooling from 24 W/m to 1 170 W/m. The change in ambient temperature did not affect the evaporative- or impingement cooling significantly. These results confirm that the implementation of evaporative cooling in the models used to calculate dynamic ratings for power lines can increase the potential current capacity significantly.

Sammendrag

Etterspørselen etter elektrisk energi er økende over hele verden. Kompleksiteten og variasjonene i både produksjon og forbruk øker også, som et resultat av flere fornybare energikilder. På grunn av denne utviklingen er det viktig å utnytte kapasiteten eksisterende kraftlinjer bedre. Tidligere har statiske grenselaster vært den vanligste måten å betjene kraftledninger på, men med ny teknologi er det blitt lettere å overvåke og bruke dynamiske grenselaster basert på målinger i sanntid av værparametere. Dynamiske grenselaster er en potensiell løsning på utviklingen i energisektoren, med de nye utfordringene som følger.

Denne oppgaven består av en litteraturgjennomgang av artikler som omhandler allerede eksisterende teknologi for måling av dynamiske grenselaster. Modellen anbefalt av CIGRE for beregning av dynamiske grenselaster er undersøkt, og er videreutviklet ved å implementere utrykk for fordampingskjøling og kjøling fra vann som dras over lederen. Hovedfokuset var å få oversikt over sammenhengen mellom endring i forskjellige værparametere og fordampningskjølingen. Hensikten med dette var å få en bedre forståelse av den potensielle mengden kjøling fra fordampning, og i hvilke værforhold og klima det kan være hensiktsmessig å implementere fordampningskjøling i modellen som brukes til å beregne dynamiske grenselaster.

Det var forventet at fordampingskjøling i stor grad var avhengig av mengden nedbør. I tillegg kom det fram av undersøkelse av modellene anbefalt av CIGRE og IEEE at omgivelsestemperatur, lederens overflatetemperatur, vindhastighet og lufttrykk også påvirker fordampningskjølingen. Resultatene fra simulering viste at med en nedbørsmengde lik 1 mm/h, og med økende vindhastighet fra 1 til 20 m/s, fører dette til en økning i fordampingskjøling fra 75 W/m til 1 368 W/m. Økning i lederens overflatetemperatur fra 10 til 80 grader, fører til en økning i fordampningskjøling fra 24 W/m til 1170 W/m. Endringen i omgivelsestemperatur påvirket ikke fordampningskjølingen- eller impingementkjøling nevneverdig. Disse resultatene bekrefter at implementering av fordampningskjøling i modellene som brukes til å beregne dynamiske grenselaster for kraftledninger, kan øke den potensielle strømkapasiteten betraktelig.

Preface

This thesis was submitted to fulfil my Master in Science degree at the Department of Electrical Power Engineering at Norwegian University of Science and Technology (NTNU), Trondheim.

I would like to thank my supervisor Erling Ildstad for sharing his knowledge with me and for guiding me through the work on this assignment. This would not have been possible without him.

It has been difficult, but at the same time interesting and exciting to work on this thesis. I have learned a lot from all the obstacles and challenges that I have encountered along the way.

June 2021

Jakob Strompdal

Table of Contents

Abstract i
Sammendrag iii
Preface v

1 Introduction **1**
1.1 Motivation 1
1.2 Project Goals 2
1.3 Structure of the report 3

2 Theoretical Background **4**
2.1 Thermal Rating 4
2.2 Static Line Rating 5
2.3 Dynamic Line Rating 6
2.3.1 Indirect measurements 7
2.3.2 Direct measurements 7
2.4 Existing Technologies 12
2.5 Calculation of the Heat Balance Equations 16
2.5.1 Parameters 16
2.5.2 Equations 18

3 Numerical Model **20**
3.1 Equation 20
3.2 Joule heating 21

3.3 Magnetic heating . . . 22
3.4 Solar heating . . . 24
3.5 Heat distribution . . . 25
3.6 Convective cooling . . . 25
3.7 Radiative cooling . . . 26
3.8 Impingement cooling . . . 27
3.9 Evaporative cooling . . . 28

4 Simulations in Matlab **29**
4.1 Background . . . 29
4.2 Simulations . . . 31
4.2.1 Wind Speed . . . 31
4.2.2 Ambient Temperature . . . 31
4.2.3 Conductor Temperature . . . 32
4.3 Assumptions and Simplifications . . . 32
4.3.1 Neglected terms . . . 32
4.3.2 Type of conductor . . . 32
4.3.3 Limitations . . . 33

5 Simple Experiment for Validation **34**
5.1 Experimental Setup . . . 34
5.1.1 Measurements . . . 35
5.1.2 Calculations . . . 37
5.1.3 Simplifications . . . 37

6 Results and Discussion **38**
6.1 Simulations . . . 38
6.1.1 Evaporative Cooling and Wind Speed . . . 39
6.1.2 Evaporative Cooling and Conductor Temperature . . . 41
6.1.3 Evaporative Cooling and Ambient Temperature . . . 43
6.2 Results from the Experiment . . . 45

7 Conclusion **47**

8 Further Work **49**

A Appendix - Monitor devices **56**
A.1 DTLR monitoring methods . . . 56

B Appendix - Calculation of parameters **57**
B.1 Magnetic core heating 57
B.2 Magnetic heating due to redistribution 57
B.3 Solar heating 59
B.4 Nusselt factor calculations 59
B.4.1 Forced convection 59
B.4.2 Natural convection 60

C Matlab **62**
C.1 Chnage in wind 62
C.2 Chnage in ambient temperature 70
C.3 Chnage in conductor temperature 77

CHAPTER 1

Introduction

1.1 Motivation

The demand for electrical power in today's society is steadily increasing. In addition, population growth and welfare increase mean that more energy generation is needed. At the same time, problems regarding climate change are more pressing than ever. As a result, conventional energy sources like oil, gas and coal are being substituted with renewable energy sources like wind, water and solar energy. In the last decade, wind farms and solar plants are often decentralized due to the need for large areas and special climate conditions. This development and more significant variations in supply and demand make it even more essential to increase the potential capacity of the power grid. Today, power lines are often operated close to their maximum limit, and conductor capacity is already a constraining factor. However, there are several ways to handle this emerging challenge.

One way is to build new power lines along the already existing lines. This is an expensive alternative and is therefore often considered undesirable. There is also possible to increase the voltage over the lines to transport more power, but this leads to stricter requirements for other components in the grid, such as transformers. This is therefore also an expensive alternative. The third

option, which will be looked into in this survey, is the possibility to increase the capacity in the already existing power lines.

Dynamic rating is a method to utilize the capacity of the power grid better. Dynamic ratings are based on external weather parameters and loading that is constantly changing. There are already done a lot of research regrading dynamic ratings, especially the impact from wind and temperature on the ratings. On the other hand, impact from precipitation is often not implemented in the models used to calculate dynamic ratings. The main focus of this thesis will be to investigate the potential impact rainfall can have on the temperature of power lines. By looking into other weather parameters that affect the cooling from rainfall, it is possible to better understand the potential contribution from this type of cooling.

1.2 Project Goals

- Get an overview of already existing technology and methods used to determine steady-state or transient ampacity and dynamic ratings on overhead power lines
- Investigate the heat balance equation, and consider what information is needed to fully utilize the potential of dynamic ratings of a power line
- Implement a model based on the heat balance equation, and perform simulation to estimate the cooling effect from water precipitation
- Evaluate and if possible, compare the result of the simulations with measurements of transient line temperatures, and discussed the validity of the methods used and the results obtained

1.3 Structure of the report

- **Chapter 2: Theoretical Background** A literature survey presenting existing technology for measuring and determining dynamic ratings.
- **Chapter 3: Numerical Model** Investigation of the heat balance equation presented by CIGRE and IEEE
- **Chapter 4: Simulations in Matlab** Presentation of model implemented in Matlab.
- **Chapter 5: Simple experiment for validation** Presentation of a simple experiment performed to investigate and validate the findings from the simulations
- **Chapter 6: Results and Discussion** Presentations of key findings from simulations performed in Matlab, and calculations from the experiment
- **Chapter 7: Conclusion**
- **Chapter 8: Further Work** Suggestions for further work is presented

CHAPTER 2

Theoretical Background

Relevant literature and work was reviewed in the project preceding this thesis. The findings from the project report is include in this Chapter. This is amended with additional knowledge, and new details have been added [1]

2.1 Thermal Rating

One possible way to solve the new challenge of increased renewable energy generation and the increase in power demand is by better utilize the potential of the already existing conductors. There are mainly two factors limiting the power network's possible power transfer today, stability- and thermal limits. In long power lines, voltage stability is often the constraining factor, while in shorter transmission lines, the thermal limit dominates. [2]

Opposite to stability limits, thermal limits are not only for reliability concerns but also for safety concerns. Primary concerns for thermal capacity are sag or annealing of power lines [2]. When conductors are exposed to high temperatures, recrystallizing can occur. The formation of crystals in the conductor change, which can lead to loss of tensile strength. [3]

The sag of a conductor is the difference between the lowest point, usually in

the middle of the line, and the point where the line is attached to a post. A certain ground clearance of the conductor must be maintained due to the potential danger of contact or electric discharges. Sag often occurs because of heating of power conductors. Heavily loaded lines can reach high temperatures leading to expansions of the conductors that are made of aluminium or copper. The heat causes the mechanical strength of the conductor to drop, which leads to more sag and less ground clearance [4]. The temperature of the conductor is highly related not only to loading but also to weather conditions and climate. Factors like solar radiation, ambient temperature, wind speed, wind direction, and rainfall affect the sag of the line.

Thermal ratings are usually divided into either static line ratings or dynamic line ratings. Static line ratings are based on "worst-case" or historical data, while dynamic ratings are based on real-time measurements of weather conditions and loading. By applying dynamic rating, it is possible to increase the current capacity in the conductor, and it will also become achievable to overload lines for a short amount of time.

2.2 Static Line Rating

Traditionally Static Line Rating has been the main way of operating power lines. Static Line Ratings are defined with the intention of not violating the upper limits of a conductors current capacity. The static line rating is based on conservative or "worst-case" weather assumptions. The same assumption is applied for the conductor all along the line. Differences in weather, wind and temperature are not taken into consideration. Static Line Rating is an easy and safe way to limit the conductors from overheating. Besides, there are no sensors or measurement devices needed along the line. [5]

CIGRE and IEEE have established a team that have developed some recommendations for base settings for the Static Line Rating. The team was called the "Joint Task Force"(JTF). For Sag-limited lines, JTF recommend a base rating for wind speed at 0.6 m/s perpendicular to the line, ambient temperature close to the annual maximum temperature along the grid, and solar radiation equal to 1000 W/m^2. For annealing limited lines, lines that

are located at narrow corridors, due to trees or buildings, JTF recommend that the base rating is set based on wind speed at 0.4 m/s or reducing the max conductor design temperature by 10°. [6]. Today static line rating is the most common way of defining the conductor capacity in the grid. Both CIGRE and IEEE states that transmission line owners or operators are free to use real-time monitoring of the weather to obtain a more suitable rating instead of the conservative Static Line Rating.

Table 2.1: SLR recommendations

	sag-limited (2019)	annealing limited
Wind	$0.6[m/s]$	$0.4[m/s]$
Temperature	max annual temp.	-
Solar radiation	$1000[W/m^2]$	-

The limits set by the JTF may be exceeded. The wind speed can be less than 0.6 m/s, the wind direction can be parallel instead of perpendicular, and the solar radiation and temperature can be higher than the recommendations. But it is unlikely that several of the assumptions are violated at the same time. The recommendations set by the JTF will provide a 99% security that the conductor temperature does not exceed the line temperature if the line current equals the line rating. [6]

The parameters the JTF have suggested are conservative, intending to maintain a safe line and grid. The Static Line ratings are therefore not the most suitable in terms of economy and conductor capacity. Maybe a better way to make use of the total line capacity is by applying Dynamic Line Rating. This is a way of monitoring real-time weather and temperature.

2.3 Dynamic Line Rating

Dynamic Line Rating is based on real-time measurements of weather, temperature and load parameters. There are many different ways to decide the

dynamic line rating limits. When choosing a measurement method, installation and maintenance costs, reliability, and performance are some of the aspects that need to be evaluated. The technologies developed for measuring real-time data can be divided into direct- and indirect measurements.

2.3.1 Indirect measurements

Indirect measurements methods focus on measuring weather conditions and parameters that affect the conductor. The conditions that are measured are used to extrapolate the value for conductor sag and minimum line clearance. The weather variations become more important if the line is lightly loaded. For heavily loaded lines, the heating from the current is the decisive factor.

Weather forecast
When deciding the dynamic rating limits, either a numerical weather model or weather forecast can be used. This is different from static line ratings, where international "worst-case scenario" standards and seasonal ratings are used. A weather model is based on numerical data that is obtained over an extended period. Based on earlier years, it is possible to predict the future weather. This method has been more reliable than the seasonal rating [7]. Weather forecast is dependent on real-time monitoring systems. Local, real-time weather data is gathered and applied to set the dynamic rating. The weather station sensors can measure parameters such as ambient temperature, wind velocity, wind angle, and solar radiation. This is a more complex way of monitoring the weather, but it makes it possible to increase the current capacity of the conductor. [2]. A critical factor when it comes to weather forecast is the ability to predict the weather one day ahead. This makes it possible to estimate better transmission line conditions.

2.3.2 Direct measurements

Direct measurement methods are based on measurements of the conductor itself. By monitoring certain properties of the conductor, it is possible to determine the capacity of the line. It is not necessary to know the weather conditions when using direct methods. Direct measurements are a more precise way, than indirect measurements, to monitor the line. There are different

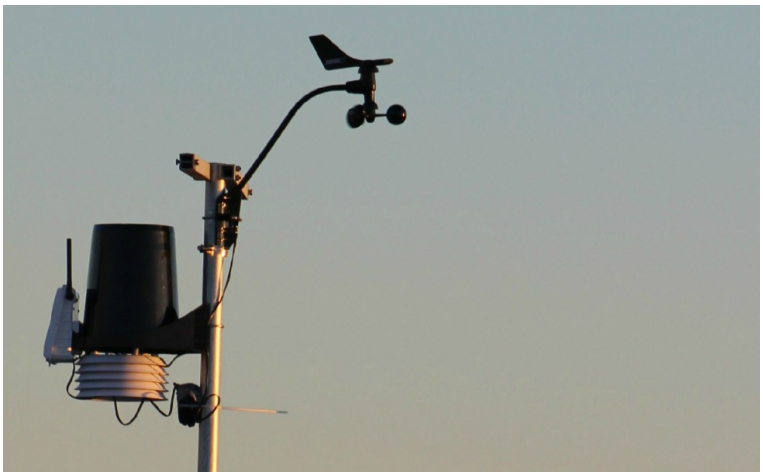

Figure 2.1: Weather station along power line

technologies than can be used. Some of the most common methods are presented below.

Temperature monitoring
Conductor temperature can either be measured at single points or over a span of the line. The temperature of the conductor can be measured to obtain information about the sag of the conductor. It is the surface temperature that is measured by the sensors, while it is the core temperature of the conductor that determines the sag. This makes the temperature monitoring systems more accurate when the line is heavily loaded [2]. In addition, the mas of the monitoring device, and the impact the device have on on the airflow can affect the conductor temperature, and cause local hot spots. This is not desirable.

For lines that are limited by ground clearance, single point temperature measurement is not optimal. The temperature can vary along the line. Therefore it is difficult to estimate the exact sag several spans away. Single spot measurement, is, on the other hand, used a lot for defining annealing of the conductor [8].

Sag monitoring
It is possible to monitor the sag of the line directly. The sag can be moni-

tored by conductor inclination, vibration frequency, target monitoring, and wave travel time [2].

A sag "stopwatch" can be used to monitor conductor sag by travelling waves. A travelling wave is initiated near the conductor clamp. The reflected mechanical wave is then measured, and it is possible to determine the conductor core temperature [8]. A field test has shown that the accuracy of the measured sag was within 0.2% [2].

Sag can also be estimated from vibration frequency. Accelerometers measure the harmonic vibration over a conductor span. The frequency's that are measured can be used to estimate conductor temperature, tension and sag. To apply this method, a minimum level of current in the conductor is needed. Some harmonics can also be affected by wind, and this can cause inaccuracy's in the measurements.

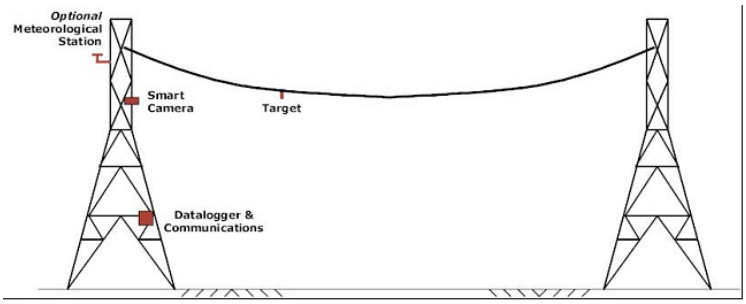

Figure 2.2: Sag monitoring of overhead power line [9]

Tension monitoring
The conductor tension can be measured at local points along the line or dead-end. The tension monitoring devices are most efficient for lines that have almost the same original tension for every span, and conductors that have high current density. The tension measured is converted into an equivalent wind speed to calculate the current capacity of the conductor based on the heat balance equation [2]. The conductor sag and the core temperature can be derived if the tension is known. Real-time tension monitoring can

measure the tension with an accuracy of 0.25% [9].

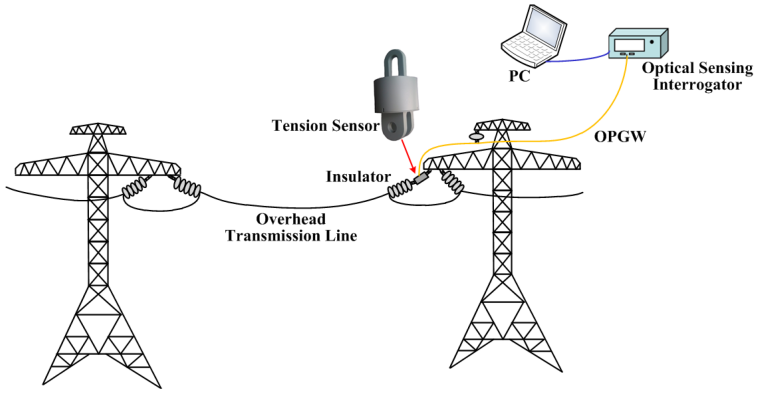

Figure 2.3: Tension monitoring of overhead power line [10]

Clearance monitoring

The clearance monitors gather information about the distance from the conductor to the ground. Acoustic waves are sent out from a device attached to the conductor. The sound waves are then reflected from the ground, and the distance to the ground objects can be gathered as a function of time. The monitors send out signals with a 10-minute interval, and the error of the data obtained is less than 1cm.

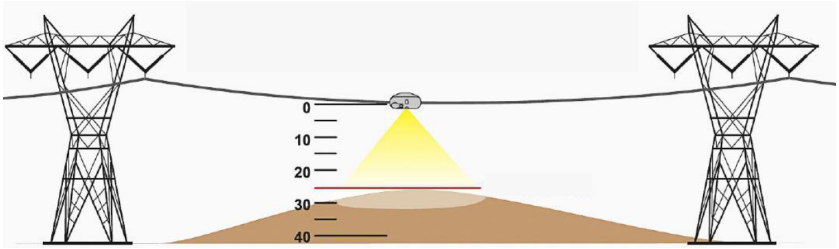

Figure 2.4: Clearance monitoring of overhead power line [11]

Angel monitoring

Angel monitoring system can be installed without power outage. Cameras placed on the towers observe the conductor tilt and sag. The tilt of the camera in relation to the conductor has to be taken into account. This method

is often used together with inclination sensors, and sensors that can measure conductor current and other parameters. LIDAR technology can also be applied to these monitoring systems [2] [8].

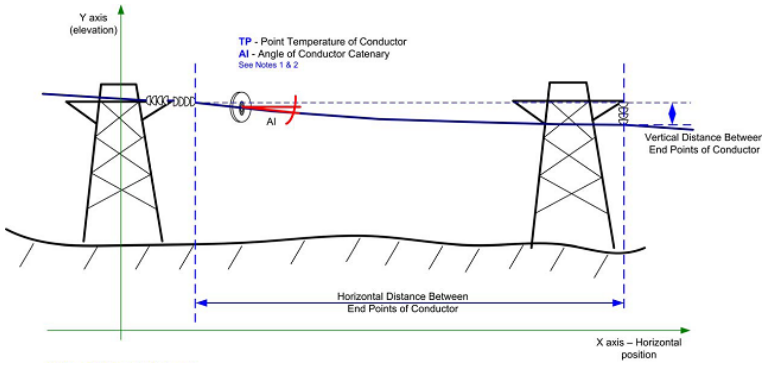

Figure 2.5: Angel monitoring of overhead power line [9]

DGPS

Differential Global Positioning System, DGPS is a more recently developed method for measuring sag of a conductor. A device attached to the conductor communicates with a GPS satellite. Information about the altitude of the device is obtained and then compared to ground level. This method has an accuracy of 25mm. There are still some challenges regarding DGPS. Factors like radio signal noise, satellite position and physical barriers for the signal can affect the operation of this system. [9]

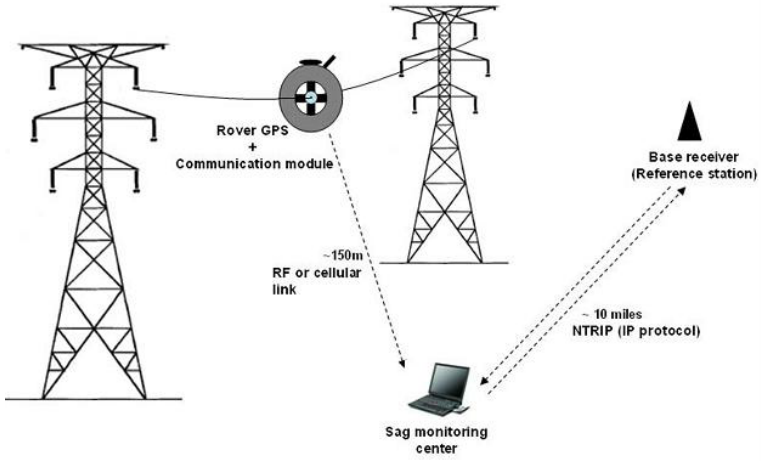

Figure 2.6: DGPS monitoring of overhead power line [9]

2.4 Existing Technologies

There are several devices that are developed for the purpose of monitoring the conductor properties mentioned above. Some devices monitor specific parameters, while most of the sensors used today have the ability to monitor several different properties.

Power Donut(USi)
The Power Donut is a monitoring device developed by USi. It can measure conductor sag, temperature and tension. It is possible to install the Power Donut on the conductor without any power outage. The Power Donut is powered by magnetic flux coupling from the conductor [12]. It can operate on all voltage levels up to 500kV.

Figure 2.7: Power Donut from USi

TLM (Lindsey)
The Transmission Line Monitoring system developed by Lindsey is able to measure conductor temperature, conductor clearance and line current and vibration, through real-time pictures. It can operate on lines up to 765kV, and it is self-powered from the current in the conductor [13].

Figure 2.8: Transmission Line Monitor from Lindsey

CAT-1(Nexans)
Nexan's CAT-1 monitor can easily be installed without power outage. The monitor is able to measure ambient parameters like temperature, solar radiation and wind. It can also give information about the line tension, of both ruling spans and dead-end structures [14] [15]. The data obtained are then used to calculate conductor clearance, sag, and real-time rating [16].

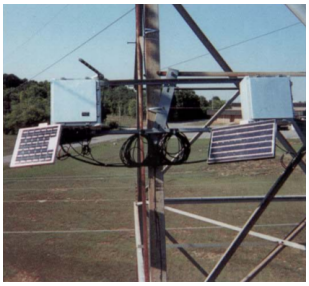

Figure 2.9: CAT-1 from Nexans [16]

ADR Sens-D (Ampacimon)
The ADR Sens-D sensor is a developed version of the ADR Sens also delivered from Ampacimon. The device computes sag from measurements of low-frequency vibration caused by wind and thermal convection [17]. The

ADR Sens-D measure the conductor current and temperature as well. The device is self-powered, light, and it can easily be installed without power outage [17]. Tests show that the Ampacimon system has a sag margin accuracy within 2% [18].

Figure 2.10: ADR Sens-D from Ampacimon [17]

Span Sentry (EDM)
The Span Sentry system consists of several sensors that can monitor conductor clearance, weather conditions and line current. The ampacity, temperature and the tension of the line can be derived from the obtained data. The system can be installed, and uninstalled, without disconnecting the line [19].

Figure 2.11: Span Sentry monitoring system from EDM [19]

OTLM sensor (OTLM, Knill group)
The OTLM sensor has the ability to measure Conductor temperature, ambient temperature, current, humidity, sag and icing. The sensor is installed

on the line and is self-powered through a current transformer [20]. The data obtained is transferred to LiMa, either via WiFi or optic cable [20].

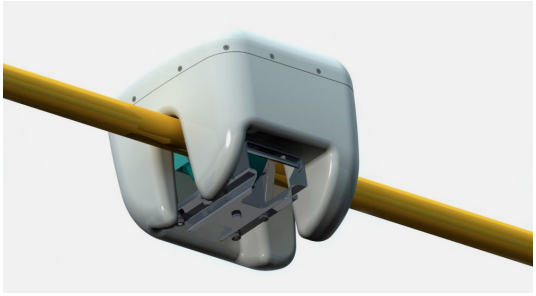

Figure 2.12: OTLM sensor from Knill Group [20]

Heimdall Neuron(Heimdall Power)
Heimdall Power is a Norwegian company that was founded in 2016. They have developed a sensor that measures critical information from overhead lines [21]. The Heimdall Neuron can measure power, line inclination, line vibration, snow load and wire temperature [22]. The Heimdall Neuron is powered from the magnetic field from the line it is attached to. It can be installed on live wires, without the need of power outage. A software called the Heimdall brain is operated beside the neuron, which uses machine learning to predict faults before they happen, and minimize the chance of blackout and failures [22].

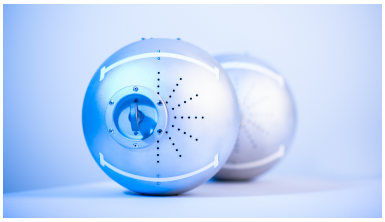

Figure 2.13: Heimdall Neuron from Heimdall Power [21]

2.5 Calculation of the Heat Balance Equations

When calculating the potential current capacity based on weather condition along the line, the heat balance equation is used. There are different variations of the heat balance equation. IEEE has developed one equation, while CIGRE uses another one. There are only minor differences between the mentioned equations.

According to IEEE the relation between current capacity and temperature is given by 2.1, [7] [23]

$$P_j + P_s = P_c + P_r \tag{2.1}$$

where P_j is the Joule heating, P_s is the solar heating, P_c is the convective cooling, and P_r is the radiative cooling.

Solar heating and the cooling can be found from measurements of incoming solar radiation, ambient temperature, and wind velocity and angle. CIGRE uses almost the same equation but adds P_M, the magnetic heating, P_i, the corona heating and P_e, the evaporative cooling. [7]. The equation used by CIGRE then become [24]

$$P_j + P_s + P_M + P_i = P_c + P_r + P_e \tag{2.2}$$

2.5.1 Parameters

P_j, Joule heating
Joule heating, also known as ohmic heating, occurs when current is flowing through a conductor. The current is converted to heat due to the resistance in a circuit. Joule heating is an undesirable effect that is a result of electric

current flow. [25]. In the heat balance equation used by CIGRE, the parameter "Joule heating" is adjusted to also take into account skin effect. [26]. For heavily loaded lines, joule heating is the main contributor to the heating of a conductor [2].

P_s, Solar heating
Solar heating is heating from solar radiation. Solar heating is dependent on the position of the sun in relation to the conductor, the latitude of the conductor, the solar declination, the time of day and the date. The impact of solar radiation is most important for lightly loaded lines. [26] [2]

P_M, Magnetic heating
Magnetic heating, also called induction heating, occurs due to cycling magnetic flux that induces eddy currents and hysteresis losses. Magnetic heating is not taken into account in IEEE's heat balance equation.

P_j, Corona heating
Corona discharges cause corona heating in a conductor. Because of ionization of air surrounding conductors, small discharges occur when the electrical field is high enough but not high enough for complete electrical breakdown. Corona discharges cause heating of the conductor. [27]

P_c, Convective cooling
Convective cooling can be separated into natural and forced cooling. Natural convective cooling is the cooling that takes place without any external impact. Forced convective cooling is mainly driven by wind. The wind speed and direction is important for the amount of heat that is transferred away. [26] [28]

P_r, Radiative cooling
Radiative cooling is the conductor's ability to remove heat through thermal electromagnetic waves. The conductor's circumferential area and impassivity are relevant for its ability to transfer heat. [28] Radiative cooling usually has a lesser impact on the heat loss than convective cooling, especially when forced convective cooling is present. [26] **P_e, Evaporative cooling**
Evaporative cooling is cooling due to evaporation of water. Rain and water vapour in the air can make the conductors wet, which causes evaporation to take place. Evaporative cooling is only considered in the heat balance equa-

tion used by CIGRE. IEEE has neglected this factor due to a small effect on the ampacity of the conductor. [26]

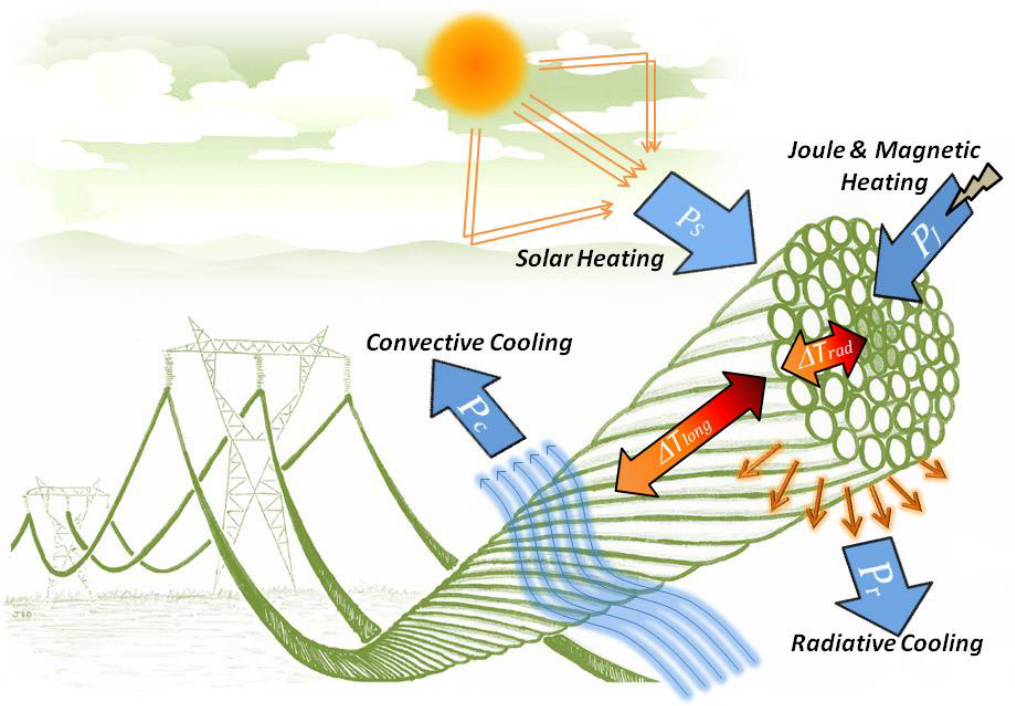

Figure 2.14: Heating and cooling of conductor, [24]

2.5.2 Equations

Steady State The heat balance equation recommended by CIGRE in "Broucuere 601", equation 2.2, depends on ambient weather parameters. The conductor is considered in steady-state when all the weather parameters remain constant [28]. When the joule heating, solar heating, magnetic heating and corona heating is equal to the convective-, radiative- and evaporative cooling, the heat balance equation can be written as

$$Heat\ gain = Heat\ loss \tag{2.3}$$

The corona heating is often neglected from equation 2.2. The corona heating can be significant at certain times, but this is usually when the wind speed is high, and in these weather conditions, the increased convective cooling will cancel the corona heating. The evaporative cooling is also neglected from CIGRE's heat balance equation. The evaporative cooling can be decisive, but it is difficult to measure, and it rare that the whole length of the line is exposed to wet conditions [28].

Equation 2.2 then becomes

$$P_s + P_M + P_i = P_c + P_r \tag{2.4}$$

This equation is often simplified even more, by considering magnetic heating as a part of joule heating. The new equation is then equal to the heat balance equation recommended by IEEE.

$$P_s + P_i = P_c + P_r \tag{2.5}$$

Transient The steady-state equation is highly simplified. In real life, the weather parameters and the load are varying with time. The conductor can, therefore, not always be considered in equilibrium, as stated in equation 2.3. CIGRE's transient heat balance equation is

$$Heat\ stored\ in\ conductor = Heat\ gain - Heat\ loss \tag{2.6}$$

The heat stored in the conductor, which is highly dependent on the properties of the material, is equal to the difference between heat gained and heat lost.

The heat gained and the heat loss is usually computed the same way in the transient state and the steady state. One way to investigate a transient case is by simulating a step change in current. The conductor is in thermal equilibrium prior to the step change, as in equation 2.14. Momentarily after the step change, the conductor temperature is unchanged, but joule heating has increased [23].

Further in this thesis, the transient state is not taken into account. The change in weather parameters is considered to have a higher impact on the conductor temperature than the inertia in the conductor in form of stored heat.

CHAPTER 3

Numerical Model

Relevant literature and work was reviewed in the project preceding this thesis. The findings from the project report is include in this Chapter. This is amended with additional knowledge, and new details have been added [1]

3.1 Equation

There are already developed numerical models for estimating the cooling contribution from precipitation on overhead power lines. By adding terms for evaporative cooling to the model based on calculations from CIGRE standard [24] it is possible to get a better understanding of the importance of precipitation.

As mentioned before, the simplified steady state model for heating of a conductor can be written as

$$q_c + q_r = q_s + q_j \tag{3.1}$$

This model is described in CIGRE [24] and IEEE [23] standards. In the paper "Dynamic Thermal Rating of Power Lines in Raining Conditions - Model and Measurements" [29] terms for rain precipitation and impinging

is added to this model to estimate the effect for evaporative cooling. The equation then becomes

$$q_c + q_r + q_e + q_{im} = q_s + q_j \tag{3.2}$$

in this section the calculation and values behind each term in equation 3.2 is presented

3.2 Joule heating

Joule heating occurs due to energy dissipated from the current flow in the conductor. The Joule heating is connected to the resistance of the conductor, and when AC is applied, the skin effect also has to be taken into account. The joule heating varies between conductors with direct current and alternate current.

Direct current
For conductor carrying direct current the joule heating is given by

$$q_j = I^2 \cdot R_{dc} \tag{3.3}$$

where

- q_j - Joule heating
- I- total direct current
- R_{dc} - direct current resistance

The resistance, R_{dc}, can be found in ana analytical way, and depends on the resistivty of the material, ρ which can be found from

$$\rho = \rho_{20} \cdot [1 + \alpha_{20} \cdot (T_{av} - 20) + \zeta_{20} \cdot (T_{av} - 20)^2] \tag{3.4}$$

where

- ρ - resistivity of a material
- T_{av} - conductor mean temperature
- ρ_{20} - resistivity at 20°

- α_{20} - linear temperature coefficient at 20°
- ζ_{20} - quadratic temperature coefficient at 20°

The quadratic term is only relevant for temperatures higher than 130°C. But it is often easier to find empirical values of R_{DC} provided by cable manufactures.

Alternating current
When operating with alternating current, a phenomenon called "skin effect" must be taken into account. The skin effect occurs when high-frequency alternating current and magnetic flux is distributed, so the density is greatest at the conductor's surface. The skin effects depend on the frequency of the current and the properties of the conductor [30]. When skin effect is present, the Joule heating can be given by

$$q_j = k_{sk} \cdot I^2 \cdot R_{dc} \tag{3.5}$$

where k_{sk} is the skin effect factor. This factor is dependent on conductor diameter and frequency. The skin effect factor can be calculated from the Bessel-function [31]. It is less accurate but a lot more effective to use a graphical method to find the value of the skin effect coefficient. Figure 3.1 shows an example of skin effect coefficients based on different conductors.

3.3 Magnetic heating

Magnetic heating is often considered as a part of the joule heating in CIGRE's heat balance equation, but if not it can be derived from

$$q_M = q_{core} + q_{redis} \tag{3.6}$$

The magnetic heating in the steal core, q_{core} occur due to alternating currents producing magnetic flux that results in power being transferred to heat because of eddy currents and magnetic hysteresis. An experimental developed equation for the magnetic core heating is

$$q_{core} = C \cdot A \cdot \gamma \cdot B_{max}^{1.83} \tag{3.7}$$

- C - constant with value of 45, at 25 °C, 290MPa and 60 Hz

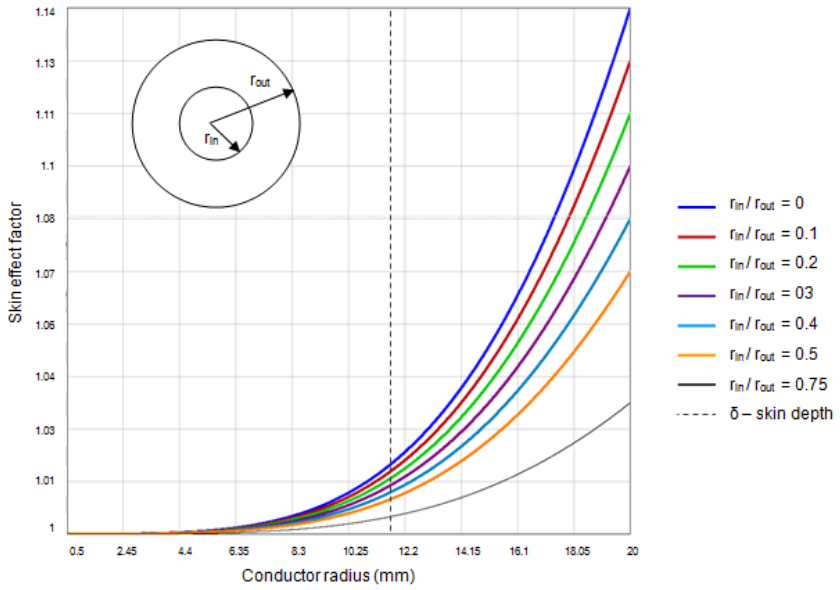

Figure 3.1: Graph that shows skin effect coefficient for different conductor radius, and the inner- ant outer radius ratio [24]

- A - cross-sectional area of the conductor
- γ - mass density
- B - magnetic induction

this equation is for systems with currents equal to 50 Hz. For other frequencies the obtained value should be multiplied by $f/60$. An alternative equation for calculating the magnetic core heating, based on the heating from unstranded wires is

$$q_{core} = 12.5 \cdot d^{\frac{1}{2}} \cdot f \cdot e^{-2.5 \cdot 10^{-3} \cdot T_c} \cdot B_{max}^{1.83} \tag{3.8}$$

The calculation of the different parameters for this equation can be found in appendix B.1.

The magnetic heat gain due to redistribution of the current densities, P_{redis} is determined by the circular and longitudinal flux in the conductor. The circular flux is not dependent on the steel core properties. It is called the skin effect and takes place in the non-ferrous layers of the conductor. The

longitudinal flux is called the transformer effect and is dependent on the steel core properties. The calculation of the impedance's of the layer of aluminium wires due to the transformer effect can be found in appendix B.2

3.4 Solar heating

The solar heating of a conductor is given by

$$q_S = \alpha_S \cdot I_T \cdot D \tag{3.9}$$

D is the outer diameter of the conductor, α_s is the absorptivity of the conductor's surface, and I_T is the global radiation intensity.

An old weathered conductor will have a α_S with a value around 0.9, while for a new conductor, the value will be around 0.2, but it is not easy not determined the α_S accurate. The absorbtivity can be estimated by determining the emissivity. The global radiation intensity, I_T, is easier to measure. This can be done by monitoring systems. The global radiation intensity consists of direct solar radiation on the surface normal to the sun, I_B, and diffuse sky radiation to a horizontal surface, I_d. I_T can therefore be written as

$$I_T = I_B \cdot (\sin(\eta) + \frac{\pi}{2} \cdot F \cdot \sin(H_S)) + I_d \cdot (1 + \frac{\pi}{2} \cdot F) \tag{3.10}$$

where F is the solar radiation reflected from the ground and H_S is the solar altitude. The solar radiation on the surface normal to the sun, at sea level, can be expressed by

$$I_{B(0)} = N_S \cdot \frac{1280 \cdot \sin(H_S)}{\sin(H_S) + 0.314} \tag{3.11}$$

where N_S is the clearness ratio, having a value of 1.0 for standard atmosphere conditions. The expression for radiation on the surface normal to the sun at any other level than sea-level, $I_{B(y)}$ can be found in appendix B.3.

There is a correlation between the radiation on a surface normal to the sunbeam and the diffuse sky radiation. The sky radiation can be written as

$$I_d = (430.5 - 0.3288 \cdot I_B) \cdot \sin(H_S) \tag{3.12}$$

3.5 Heat distribution

The heat in an operating conductor is not evenly distributed. Both radial and axial variations in temperature are common. This will affect the resistance and the further joule heating of the line. The cooling from convection and radiation depends on the conductor's surface temperature, while the sag and annealing of conductors are more dependent on the core temperature. The heat distribution is different for different types of conductors. For a cylindrical conductor with a core consisting of a different material, the heat distribution can be modelled as [24],

$$T_c - T_s = \frac{P_T}{2\pi\lambda} \cdot \left(\frac{1}{2} - \frac{D_1^2}{D^2 - D_1^2} \cdot \left(\ln \frac{D}{D_1} \right) \right) \tag{3.13}$$

where

- λ - radial thermal conductivity $[W/m \cdot K]$
- P_T - total heat gain $[W/m]$
- D - outer diameter $[m]$
- D_1 - internal diameter (steel core) $[m]$

For a mono metallic conductors like AAC, D_1 is equal to zero, and the equation can be simplified to

$$T_c - T_s = \frac{P_T}{4\pi \cdot \lambda} \tag{3.14}$$

3.6 Convective cooling

Convective cooling is an essential part of the cooling of overhead transmission lines. Convective cooling can be divided into natural and forced cooling. Natural convective cooling occurs at zero wind speed, while forced convective cooling occurs when the wind speed is different from zero. The forced cooling is dependent on wind speed and the wind angle relative to the conductor. The thermal rating of a conductor is rarely violated if convective cooling is high.

It is difficult to calculate and determine the cooling effect from the wind on the conductor. This is because the wind speed and wind angle differ along the line, and the heat of the conductor is not evenly distributed. There are some methods for calculating the cooling that is based on statistical analysis that is under development.

The heat transfer, or cooling, from a conductor to the surroundings can be expressed as

$$q_c = \pi \cdot \lambda_f \cdot (T_S - T_a) \cdot Nu \tag{3.15}$$

where

$$\lambda_f = 2.2368 \cdot 10^{-2} + 7.23 \cdot 10^{-5} \cdot T_f - 2.763 \cdot 10^{-8} \cdot T_f^2 \tag{3.16}$$

- λ_f is the thermal conductivity of air at T_f
- T_f is the temperature of the air in contact with the surface of the conductor
- T_s is the temperature of the conductor surface
- T_a is the temperature of the air
- Nu is the dimensionless Nusselt number [32]

T_f is often assumed to be $= 0.5 \cdot (T_s + T_a)$.

The Nusselt factor is an important part of the equation, and it is therefore important to choose the correct value for this factor. The Nusselt factor is dependent on wind factors like speed, angle and turbulence. CIGRE's suggestions for how to determine the value of the Nusselt factor can be found in appendix B.4.

3.7 Radiative cooling

The radiative cooling, or radiative heat loss, of a conductor is energy that is transmitted through the surface of the conductor. Radiative cooling can be divided into, radiation to ground and surroundings, and radiation to the sky. The Stefan-Boltzman law describes the heat loss due to radiation

$$\begin{aligned} q_r = &\pi \cdot D \cdot \sigma_B \cdot \mathcal{F}_{c-g} \cdot \epsilon_s \cdot [(T_s + 273)^4 - (T_g + 273)^4] + \\ &\pi \cdot D \cdot \sigma_B \cdot \mathcal{F}_{c-sky} \cdot \epsilon_s \cdot [(T_s + 273)^2 - (T_{sky} + 273)^4] \end{aligned} \tag{3.17}$$

where

- D is the outer diameter
- σ_B is the Stefan-Boltzmann constant
- ϵ_s is the emissivity of the surface of the conductor
- T_s is the temperature of the conductor surface
- T_g is temperature of the ground
- T_{sky} is the temperature of the sky
- $\mathcal{F}_{c-g}$ is the fraction of radiated energy from conductor to ground
- $\mathcal{F}_{c-sky}$ is the fraction of radiated energy from conductor to the sky

It is often possible to set T_g and T_{sky} equal to the ambient temperature, T_a, which is easier to estimate In addition $\mathcal{F}_{c-g}$ and $\mathcal{F}_{c-sky}$ can be set equal to one. Equation 3.17 then becomes

$$q_r = \pi \cdot D \cdot \sigma_B \cdot \epsilon_s \cdot [(T_s + 273)^4 - (T_a + 273)^4] \tag{3.18}$$

Radiative cooling has much more impact when the conductor temperature is high. Nevertheless, it has usually less impact than convective cooling.

3.8 Impingement cooling

Impingement cooling is cooling due to water or precipitation flow over the surface of the conductor. The impingement cooling can be described as

$$q_{im} = \frac{0.71}{\pi} \cdot c_w \cdot f_p \cdot (T_S - T_a) \tag{3.19}$$

where t_S is the skin temperature of the conductor, T_a is the ambient temperature, and c_w is the specific heat capacity of water. The equation also contains the rain mass flux which can be modelled as

$$f_p = \sqrt{\left(\frac{10^{-3}}{3600} P \cdot \rho_w\right)^2 + (u \cdot 6.710^{-5} \cdot P^{0.84})^2} \tag{3.20}$$

where u is the wind velocity, P is the precipitation rate and ρ_w is the water density [29].

3.9 Evaporative cooling

The contribution from evaporative cooling when water vapour and droplets only are presented in the humid air is not significant. It can be a significant factor when the conductor is wetted from rain [26]. CIGRE states that this parameter is neglected because it is rare that the whole line is wet from rain at the same time, and it is difficult to assess [24]. The contribution from evaporative cooling can be modelled as

$$q_e = -W_f \cdot f_e \cdot L_e \tag{3.21}$$

where W_f is the wetted factor of the power line, f_e is the evaporative mass flux, and L_e is is the latent heat for evaporation, equal to $2260[kJ/kg]$. The rain mass flux can be modelled as

$$f_e = \frac{k \cdot h}{c_p} \cdot \left(\frac{(1-r)e_s}{p} \right) \tag{3.22}$$

where c_p is the specific heat of air. p is the air pressure, k is the ratio of molecular weights of water vapour and dry air, which is equal to 0.62 [29]. e_S is the saturation pressure equal to

$$e_s(T) = e_{s0} \cdot e^{\left(\frac{L_e}{R_v}\left(\frac{1}{T_0} - \frac{1}{T}\right)\right)} \tag{3.23}$$

where e_{s0} is equal to 6.1hPa and R_v is 461J/kgK. h is the heat transfer coefficient. At last it can be noted that the maximal amount of evaporated water, evaporation mass flux, can not be higher than the impinging mass flux. The wetted factor W_e is often considered to be constant with value between 0.5 and 1.0, but can also be modelled as a factor deepened on the rain mass flux and the precipitation rate [29]

$$W_f = \frac{arctan(1600 \cdot f_p)}{\frac{\pi}{2} + 1.6} \tag{3.24}$$

CHAPTER 4

Simulations in Matlab

4.1 Background

The main object of this thesis was to study and consider the possible benefit of implementing evaporative cooling in models for calculating dynamic ratings. It is difficult to compute the exact impact of evaporative cooling on a heated overhead conductor. Both CIGRE [24] and IEEE [23] states that the cooling impact from evaporation of water or precipitation can be of significant value, but it is difficult to assess [26]. The cooling from evaporation due to rainfall is dependent on several factors. The amount of water that hits the line and the size of the water droplets, the air temperature and pressure, and the conductor temperature are all important factors that have to be evaluated to estimate the contribution from this type of cooling. The contribution from evaporative cooling when water vapour and droplets only are presented in the humid air is not significant. However, it can be a significant factor when the conductor is wetted from rain [26].

The cooling effect from evaporation is not only dependent on the precipitation. By looking at the equations presented in Chapter 3.1, Numerical model, it is clear that other variables like wind speed, air pressure, and temperatures affect the amount of cooling from evaporation. The intention of

these simulations is to get an overview of which parameters, other than precipitation rate, that have an impact on the evaporative cooling effect. By isolating certain parameters, it is, therefore, possible to get a better understanding of each single parameters contribution to the overall cooling.

Equation 3.21, for evaporative cooling is replicated below.

$$q_e = -W_f \cdot f_e \cdot L_e \tag{4.1}$$

It can be seen that evaporative cooling, e_q is directlig depend on

- Wetted factor, W_f
- Evaporative mass flux, f_e
- Latent heat for evaporation, L_e

Further, these factors are depended on other weather parameters. Figure 4.1 shows variables that affect the evaporative cooling.

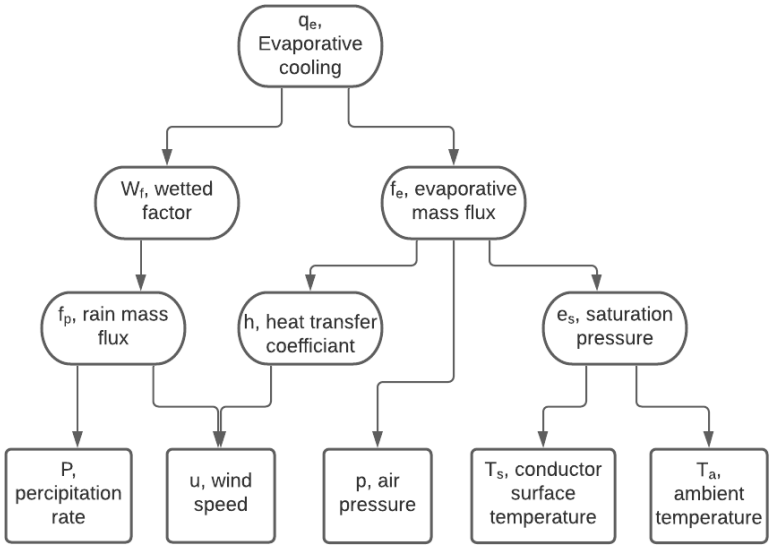

Figure 4.1: Sketch of variables that affect the evaporative cooling on a conductor

4.2 Simulations

As can be seen from figure 4.1, that precipitation rate, wind speed, air pressure, ambient- and conductor temperature are all factors that affect evaporative cooling. Therefore, in addition to precipitation rate, wind speed, ambient temperature and conductor temperature will be investigated in the simulations. On the other hand, the air pressure is not a focus in the simulation because it is almost constant and will probably not significantly affect evaporative cooling. The Matlab script can be seen in Appendix C.

4.2.1 Wind Speed

The wind speeds impact on the evaporative cooling is investigated by keeping other variables constant, and then change the amount of wind speed. The wind is alternated from 1 m/s to 20 m/s with a step length of 1. The other weather parameters and the current is initially set to

- Current, $I = 1000[A]$
- Ambient temperature, $T_a = 10[C^\circ]$
- Surface temperature of conductor, $T_S = 40[C^\circ]$
- Clearness ratio, $N_s = 0$

4.2.2 Ambient Temperature

The evaporative cooling dependency on ambient temperature is investigated by changing the temperature from 1 C° to 30 C°, while other parameters are give the initial value

- Current, $I = 1000[A]$
- Wind speed, $u = 1[m/s]$
- Surface temperature of conductor, $T_S = 40[C^\circ]$
- Clearness ratio, $N_s = 0$

The cooling of the conductor is not investigated for temperatures below zero degrees. This is explained later under limitations, 4.3.3.

4.2.3 Conductor Temperature

The conductor surface temperature is changed from 1 C° to 80 C° with a step length equal to 1. The other variables are initial set to

- Current, $I = 1000[A]$
- Wind speed, $u = 1[m/s]$
- Ambient temperature, $T_a = 10[C^\circ]$
- Clearness ratio, $N_s = 0$

4.3 Assumptions and Simplifications

4.3.1 Neglected terms

Magnetic heating
The term for magnetic heating presented in Chapter 3.1 is not implemented in the Matlab simulations. However, the skin effect implemented in the term for joule heating covers some of the magnetic heating. The contribution from the neglected term is not significant and has no impact on the contribution from the evaporative cooling, which is the focus in these simulations.

Solar heating
The term for solar heating is also neglected in the simulations. As mentioned, the simulations are performed to get an overview of cooling from evaporation. Evaporative cooling is dependent on precipitation. For simplicity is the "clearness ratio" set to zero when there is precipitation present. It is assumed that when it rains, there are many clouds, and the solar radiation is equal to zero. In reality, the solar radiation will be close to zero and will not affect the total heating of a conductor.

4.3.2 Type of conductor

Different types of conductors have different properties. The diameter of the conductor and the material of the conductor affect the contribution from evaporative cooling. Some common conductors used for high-voltage transmission lines is ACSR(Aluminium Conductor Steel Reinforced) and

AAAC(All Aluminium Alloy Conductor). The conductor type is set to be an AAAC conductor in the simulations performed due to a more straightforward calculation procedure. If simulation over an ACSR conductor is desirable, a new term for calculating the resistance must be included. The ACSR consist of both steel and aluminium, and different diameters have to be taken into account.

The simulations are performed over a conductor with following properties

- Diamter, $D = 0.02[m]$
- Skin effect fator, $k_{sk} = 1.08$
- Temperature coefficiant, linear, $\alpha = 0.0042[1/K]$
- Temperature coefficicant, quadratic, $\zeta = 8 \cdot 10^{-7}[1/K^2]$
- Resistivity of aluminium at 20 degrees, $\rho_{20} = 2.65 \cdot 10^{-8}$

4.3.3 Limitations

The simulations performed for investigating evaporative cooling are only valid for precipitation in the form of rain, not snow. There is a significant difference in cooling from snow compared to rain. When calculating evaporative cooling from precipitation in the form of snow, the heat needed for the phase change from snow to water has to be evaluated in addition to the heat absorbed from the phase change water to gas. Snow also occur in a different density and weight than rain, and the equation 3.21 is therefore not valid for calculating evaporative cooling from snow. Therefore, the results from the simulations will only show the heating for ambient temperatures down to zero degrees.

CHAPTER 5

Simple Experiment for Validation

In this Chapter, the contribution from evaporative cooling will be investigated by calculations based on rough estimations of precipitation and conductor temperatures and already know thermodynamic laws. These results will not give an exact answer but can give an understanding of the contribution from evaporative cooling on power lines. This experiment will neither confirm nor infirm the results from the simulations but can increase or decrease the validity. The experiment is performed with little test equipment available, but a proposal on how to increase the scope of the experiment will also be presented.

5.1 Experimental Setup

An initial experiment was performed to understand the importance of evaporative cooling from precipitation on an overhead conductor. The reason for this experiment was not to determine specific values or make any major conclusions but to determine if it is possible that evaporative cooling can have a significant effect on power lines.

In rainy conditions, water and water vapour will penetrate into air pockets between the strands of the conductor. This water will potentially evaporate

and contribute to a cooling effect. The amount of water that sticks to the conductor and evaporate is highly dependent on the type of conductor. A stranded conductor with several layers will naturally absorb more water than a solid or a composite conductor. By investigating the amount of water that will stick to the conductor, it is possible to roughly estimate the heat energy used to evaporate the water.

5.1.1 Measurements

Equipment used

- ACSR 26/7
- Container with water
- Scale

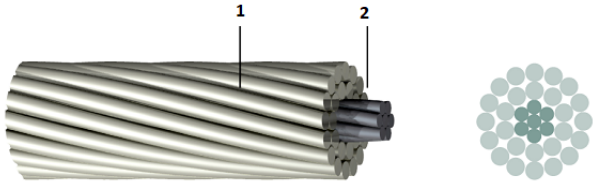

Figure 5.1: ACSR 26/7 [33]
1 - Aluminium layers
2 - steel core

An ACSR 26/6 conductor with two layers of aluminium strands surrounding a steel core, were used in this experiment, shown in Figure 5.1. First, the weight of the conductor was measured on a scale. Then the conductor was put in a container filled with water. Some of the air pockets between the strands were filled with water, and the weight of the conductor was then measured again. The meaning of this was to get a estimate of the volume between the strands, and the amount of water that potentially could be exposed to evaporation.

Figure 5.2: Conductor before put into water. Weight: 223g

Figure 5.3: Conductor after put into water. Weight: 238g

5.1.2 Calculations

By using the specific heat equation and the data obtained from the simple experiment, it is possible to estimate some rough calculations regarding the evaporative cooling of ACSR 26/7. The specific heat equation is presented below.

$$Q = c \cdot m \cdot \Delta\Theta + m \cdot L_v \tag{5.1}$$

The equation consist of two parts. The first is called the sensible heat and describes the energy needed to raise the temperature of the substance. This part of the term consists of c - the specific heat capacity of a substance, m - the mass, and $\Delta\Theta$ - the temperature change. The second part is called the latent heat and describes the heat needed for the phase change and consists of L_v - the latent heat, and m - the mass.

5.1.3 Simplifications

When calculating the amount of heat obtained from the evaporation of water on the conductor several assumption and simplification has been made. The temperature change does not affect the specific heat of either water or aluminium throughout the calculations. Specific heat of water is set to 4.2 kJ/kW·K, and specific heat of aluminium is set to 0.9 kJ/kW·K. In addition, evaporation of water on the conductor will happen for all temperatures, depending on the saturation of the surrounding air. Nevertheless, in these calculations, it is assumed that evaporation only happens when the water reaches the temperature of the conductor. The conductor consists of aluminium and steel, but it is assumed that only the aluminium "carrying" the heat; therefore, heat exchange only happens between water and aluminium.

CHAPTER 6

Results and Discussion

6.1 Simulations

The results from the Matlab simulation are presented and disgusted in this chapter. The effect wind speed, ambient temperature, and conductor temperature have on evaporative cooling will be evaluated.

In the graphs obtained from Matlab, some parameters occur. q_j is the joule heating, q_r is the radiative cooling, q_c is the convective cooling, q_i is the impingement cooling, and q_e is the evaporative cooling. All these terms are presented in Chapter 3.1. Further the term q_1 and q_2 occur. q_1 is the overall heating, while q_2 is the total heating without the evaporative- and impingement cooling.

$$q_1 = q_j + q_r + q_c + q_i + q_e \tag{6.1}$$

$$q_2 = q_j + q_r + q_c \tag{6.2}$$

6.1.1 Evaporative Cooling and Wind Speed

Figure 6.1 shows the overall heating of a conductor for different wind speeds. In the red graph, q_2, is the contribution from evaporative cooling and impingement cooling neglected. The blue graphs show the total heating, including evaporative cooling and impingement cooling, with different precipitation amounts. Each blue line is for precipitation from 1 mm/h to 10 mm/h.

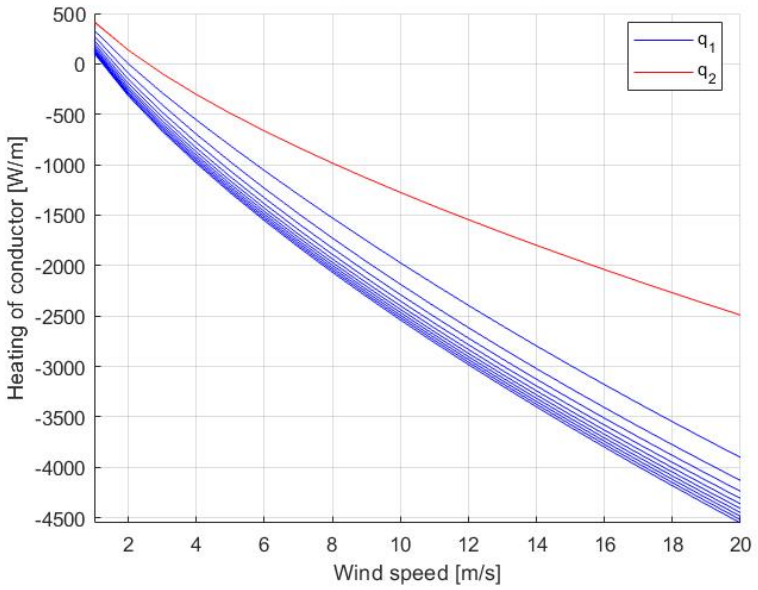

Figure 6.1: Overall heating of a conductor as a function of wind speed. q_1 is the term including evaporative.- and impingment cooling. q_2 is the term without evaporative.- and impingment cooling

It can be seen from Figure 6.1 that the difference in the heating of q_1 and q_2 for low wind speeds is lesser than the difference at high wind speeds. For wind speed equal to 1 m/s the q_2 heating is equal to about 400 W/m, while the heating for q_1 with P=1 is about 300 W/m, and q_1 with P=10 is about 100 W/m. The evaporative- and impingement cooling contributes with 100 to 200 W/m. For wind speed equal to 20 m/s the difference is much greater. At this wind speed q_2 is equal to -2500 W/m while q_1 i between -3800 and -4500 W/m. The contribution from evaporative- and impingement cooling is then around -2000 W/m.

It can be seen that the graph flattens out as the wind speed is increased. The increase in cooling is lesser at high wind speeds than at low wind speeds. Looking at Figure 6.2a and Figure 6.2b it can be seen that the reason for this development is primarily because of the contribution from the convective cooling and not the evaporative cooling. Convective cooling and evaporative cooling are the only terms noticeable affected by the change in wind speed. From Figure 4.1 it can be seen that the wind speed affect both the evaporative mass flux and the rain mass flux, which both affect the evaporative cooling. The rain mass flux is affected by the rain because a change in the wind will affect the amount of rain dragged across the conductor. However, by looking at the impingement cooling, it can be seen that this contribution does not make any significant difference. On the other hand, the wind speed is highly affecting the evaporative mass flux. This is because the wind will transport saturated air away from the conductor.

Maybe the most important observation from Figure 6.1 is that the actual amount of precipitation is less important than that it is precipitation present. The difference of cooling if the precipitation is 0 and 1 mm/h is much greater than the difference if precipitation is 9 and 10 mm/h, especially at high wind speeds.

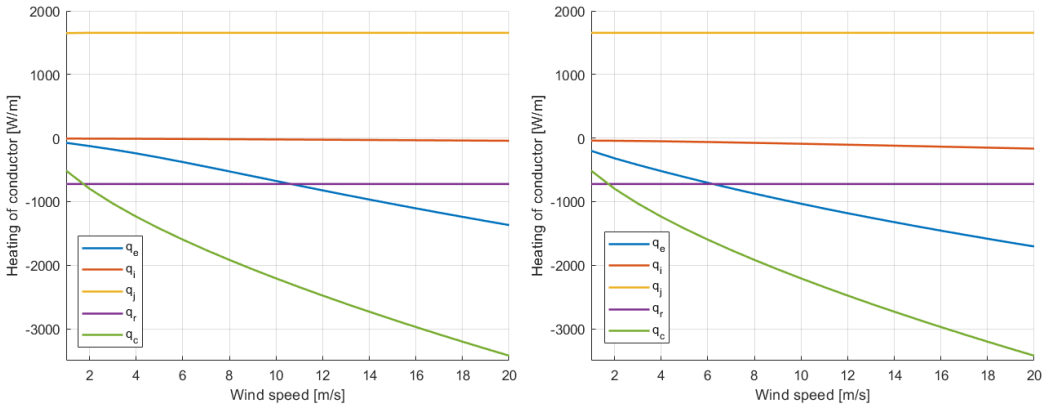

(a) P=1 (b) P=5

Figure 6.2: Change in heating for different terms as a function of wind speed

6.1.2 Evaporative Cooling and Conductor Temperature

Figure 6.3 shows the overall heating for different conductor surface temperatures. Like Figure 6.1 the blue lines shows the overall heating for a different amount of precipitation. In contrast, the red line is the heating where evaporative- and impingement cooling is not taken into account.

The heating of the conductor is decreasing as the conductor temperature is increasing, as can be seen in Figure 6.3. This simulation is not meant to show an actual physical development of the heating of the conductor. In reality, the increase of conductor temperature occurs because of a change in weather or increased current in the conductor. In this simulation, the current is kept constant, and the graph is just for showing the impact from the cooling terms at different temperatures. As expected, the cooling from convective cooling, water evaporation, and radiative cooling to the surroundings is increasing as the conductor's temperature increases.

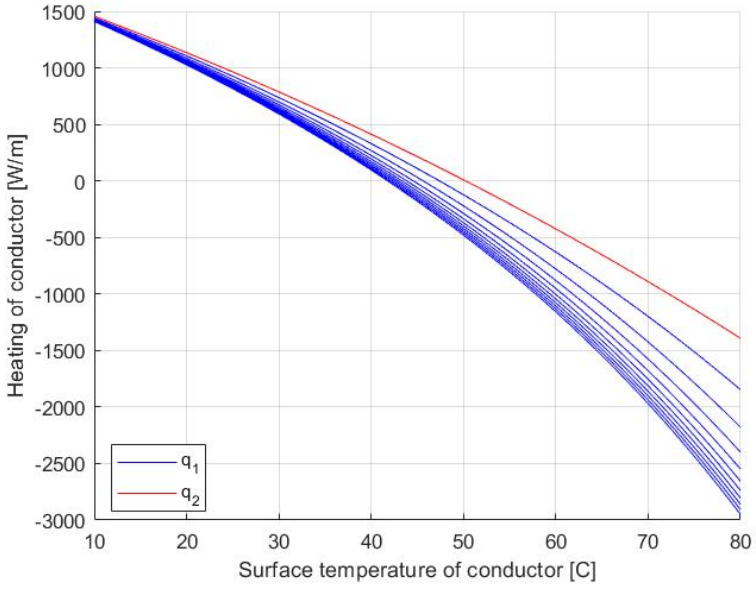

Figure 6.3: Overall heating of a conductor as a function of conductor surface temperature. q_1 is the term including evaporative.- and impingment cooling. q_2 is the term without evaporative.- and impingment cooling

It can be seen that at conductor surface temperature equal to $10C^{\circ}$ the difference between the lines in Figure 6.3 is nothing. This is because of a simplification in the model, where the rain temperature is set to be equal to the ambient temperature. In this simulation the ambient temperature is set to $10C^{\circ}$, 4.2.3. The rain will therefore not contribute to any cooling effect. At $80C^{\circ}$ the contribution from evaporative- and impingement cooling can be seen. There is also a noticeable difference between cooling for a different amount of precipitation.

In Figure 6.4a and 6.4b it can be seen that radiative cooling is the greatest cooling source for all the conductor temperatures, followed by convective cooling. The cooling from radiation and convection is relatively linear, while evaporative cooling increases exponentially as the conductor temperature increases. With a greater amount of precipitation and an even higher conductor temperature, it is likely to believe that the contribution from evaporative cooling will precede the convective cooling and maybe also match the contribution from radiative cooling.

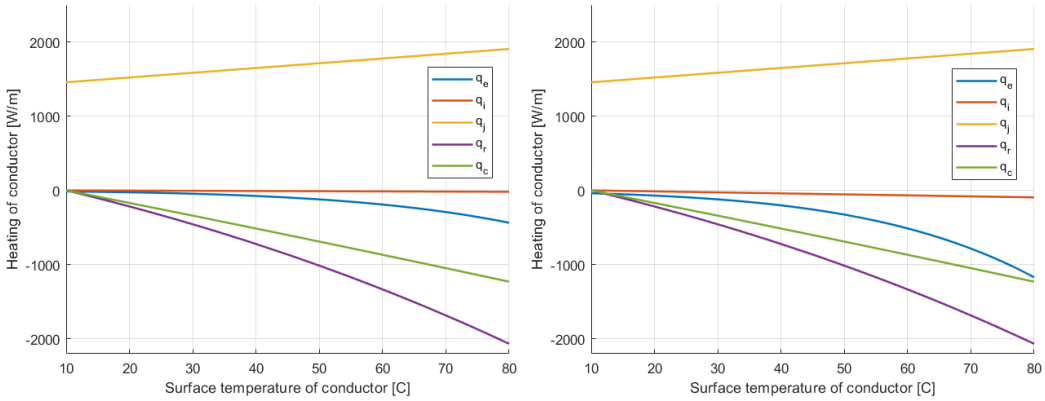

(a) P=1 (b) P=5

Figure 6.4: Change in heating for different terms as a function of conductor surface temperature

6.1.3 Evaporative Cooling and Ambient Temperature

Figure 6.5 shows the heating development for increasing ambient temperature. As expected, higher ambient temperatures cause more significant heating of the conductor. The heating is almost linearly increasing, unlike the results in earlier simulations. The evaporative cooling with precipitation rate equal to 1 mm/h contributes with cooling at around 100 W/m. This applies for all ambient temperatures. The cooling is, of course, greater for a higher amount of precipitation, but the difference in cooling between P=1 and P=2 is greater than the difference between P=9 and P=10.

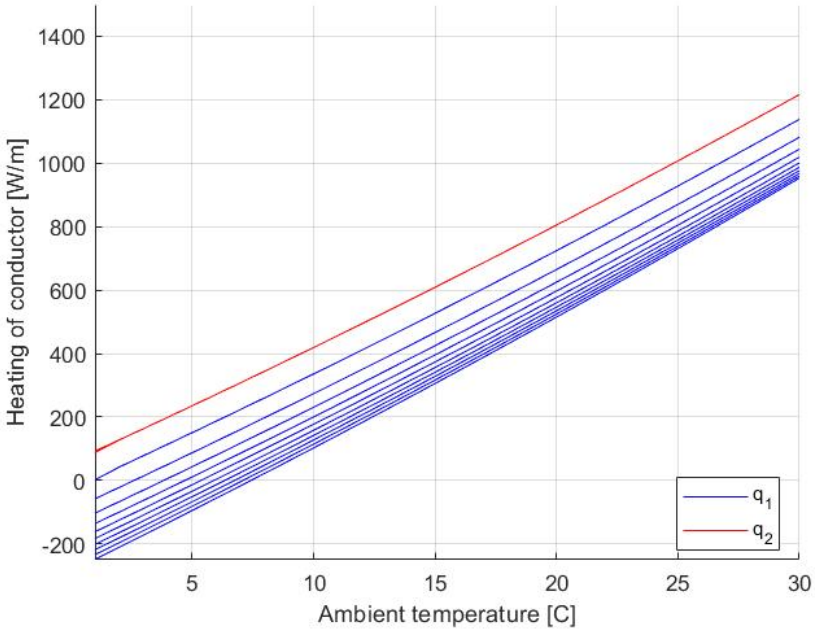

Figure 6.5: Overall heating of a conductor as a function of ambient temperature. q_1 is the term including evaporative.- and impingment cooling. q_2 is the term without evaporative.- and impingment cooling

From Figure 6.6a and Figure 6.6b it can be observed that the evaporative cooling and impingement cooling is almost constant for every ambient temperature. The increase in heating seen in Figure 6.5 is due to the decrease in cooling from convective and radiative cooling. The development shows that

for ambient temperatures equal to $30C°$, and precipitation rate higher than 5 mm/h, evaporative cooling will stand out as the essential cooling source.

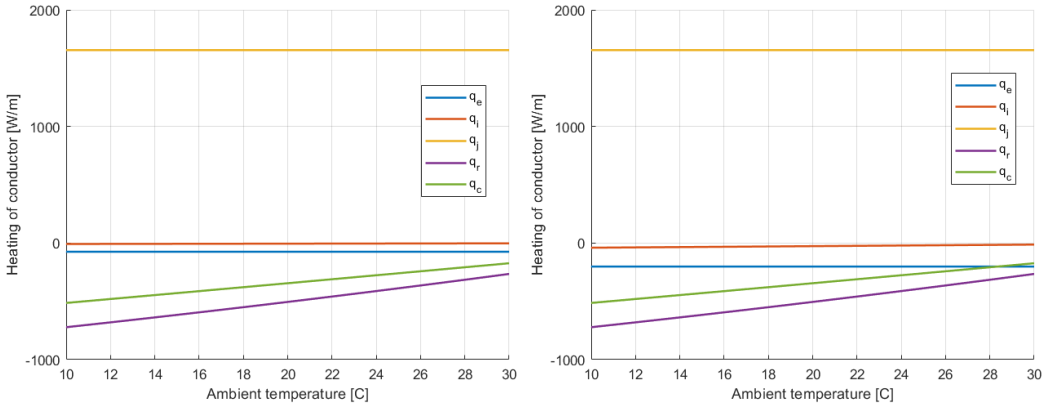

(a) P=1 (b) P=5

Figure 6.6: Change in heating for different terms as a function of ambient temperature

6.2 Results from the Experiment

The experiment The values used in the calculation is presented in the table below

Variable		values	
m_W	Mass of water	0.015	kg
m_{Al}	Mass of aluminium	0.223	kg
c_W	Specific heat of water	4.2	$\frac{kJ}{kg \cdot K}$
c_{Al}	Specific heat of aluminium	0.9	$\frac{kJ}{kg \cdot K}$
L_v	Latent heat vaporization, water	2 260	$\frac{kJ}{kg}$
Θ_c	Temperature of conductor	80	C°
Θ_i	Initial temperature of water	10	C°
Θ_v	Temperature of water when evaporated	80	C°

Table 6.1: Caption

By inserting the values presented in table 6.1 values into equation 5.1 it is possible to get an impression of the effect of cooling from rainfall on the conductor. The result obtained by this approach will likely be higher than the actual cooling because the evaporation of water will occur evenly distributed over the temperatures as it gets heated up, and not all at $80C^\circ$. It can therefore be assumed that the amount of evaporative cooling will be slightly less than the Q_1 in equation 6.3.

$$Q_1 = m_W \cdot L_v \tag{6.3}$$

$$Q_2 = c_W \cdot m_W \cdot \Delta\Theta_W \tag{6.4}$$

Equation 6.4 shows the calculation of the heat obtained without the evaporation, only the heating of the water; this is called impingement cooling. On the other hand, equation ref 6.3 shows the calculation for the heat obtained from evaporation of the water.

Inserting values from Table 6.1 the value is

$$Q_1 = 2.4 \cdot 0.015 \cdot (80 - 10) + 0.015 \cdot 2260 = 33.90[kJ] \tag{6.5}$$

$$Q_2 = 2.4 \cdot 0.015 \cdot (80 - 10) = 2.52[kJ] \tag{6.6}$$

From the simulations, with precipitation equal to 5 m/s and conductor temperature equal to 80 C°, the cooling effect per meter for evaporation is equal to 1170.8, while for impingement, it is 93.92. The relationship, evaporative cooling over impingement cooling, is then 12.54. The relationship between the values calculated from the specific heat equation in the experiment is 13.45. The two relationships, from the simulations and the experiment, is pretty similar.

It is difficult to find other similarities between the experiment and simulations that will validate the model used in the simulations. To estimate the effect in Watt from the experiment, the time it takes for the water to evaporate have to be known. By reversing the calculation we can find that

$$[W] = [J/s] \Rightarrow [s] = [J/W] \tag{6.7}$$

$$t = \frac{36900[J]}{1170.8[W]} = 31.5[s] \tag{6.8}$$

The statement that it will take 31.5 seconds to evaporate the water in the experiment is only a wild guess. This can be confirmed or disproved by applying current to the conductor and further experiments.

CHAPTER 7

Conclusion

The conclusion of the literature review and the simulations performed are summarized in these bullet points.

- The use of dynamic ratings to utilize more of the potential transmission capacity in power lines is increasing. Several different technologies for measuring real-time weather parameters are available on the market.
- The choice of monitoring device depends on the location of the power line being monitored. Conductors located in narrow corridors, due to vegetation or buildings, are more exposed to annealing, while for power lines in open areas, sag is often the limiting factor.
- Evaporative cooling and impingement cooling is often neglected from models used to calculate dynamic ratings. This is because it can be difficult to assess or because it is considered to have a low impact on the overall heating of the conductor.
- It is not only the precipitation rate that affects the evaporative cooling. Evaporative cooling is also affected by wind speed, conductor surface temperature, ambient temperature and air pressure. The air pressure

is almost constant, but variations in wind speed and temperatures are important when calculating the evaporative cooling on a conductor.

- It is a greater amount of evaporative cooling at high wind speeds and high conductor temperatures, while ambient temperature does not significantly impact the cooling from evaporation.
- Evaporative cooling has, more often than not, a lower contribution to the overall cooling than convective cooling and radiative cooling. Nevertheless, in certain weather conditions, evaporative cooling can be of importance for overall cooling.
- Impingement cooling is very often negligible because it contributes to a tiny per cent of the overall cooling.

CHAPTER 8

Further Work

Based on the results and discussion suggestions for further work is:

- The simulations are performed for a very limited set of scenarios. Wind speed, ambient- and conductor surface temperature are investigated separately. It could be interesting to investigate evaporative cooling when several weather parameters are changed at the same time.
- The experiment performed gives an estimate and impression of possible cooling from evaporation, but it does not confirm the results from the model. By applying current to the conductor, it should be possible to validate the results from the simulations.
- The results from the simulations should also be compared to real-time measurement of evaporative cooling on existing power lines at certain weather conditions
- The model recommended by CIGRE is investigated in this thesis. The model recommended by IEEE is also looked into, but to get an even better understanding of the correlations and difference the model recommended by IEC should also be considered.
- The model used for the simulations is simplified. To obtain a more exact

result, terms for solar heating, magnetic heating and corona heating can be added.

Bibliography

[1] J. Strompdal, "Thermal rating of overhead power lines-a comparison of cigre and ieee standards for calculation of thermal ratings," Dec. 2020.

[2] S.Karimi, P.Musilek, and A.M.Knight, "Dynamic thermal rating of transmission lines: A review," Renewable and Sustainable Energy Reviews, Volume 91, August 2018, Pages 600-612, 2018.

[3] V. T.Morgan, "The loss of tensile strength of hard-drawn conductors by annealing in service," IEEE Transactions on Power Apparatus and Systems, Vol. PAS-98, No.3, 05 1979.

[4] R.Lijia, L. Hong, and L. Yan, "On-line monitoring and prediction for transmission line sag," IEEE International Conference on Condition Monitoring and Diagnosis, 09 2012.

[5] I.Albizu, E.Fernandez, R. M.T.Bedialauneta, and A.J.Mazon, "Adaptive static line rating for systems with htls conductors," IEEE Transactions on Power Delivery, °arg. 33, nr. 6, 2018.

[6] W. group B2.12, "Guide for the selection of weather parameters for bare overhead conductor ratings," CIGRE TB, 2006.

[7] P. H. Kateryna Morozovska, "Study of the monitoring systems for dynamic line rating," Energy Procedia Volume 105, pages 2557-2562, 05 2017.

[8] C.R.Black and W.A.Chisholm, "Key considerations for the selection of dynamic thermal line rating systems," IEEE TRANSACTIONS ON POWER DELIVERY, VOL. 30, NO. 5, 2015.

[9] W. G. B2.36, "Guide for application of direct real-time monitoring systems," TB-498, 06 2012.

[10] G. ming Ma, Y. bo Li, N. qiang Mao, C. Shi, B. Zhang, and C. rong Li, "A fiber bragg grating-based dynamic tension detection system for overhead transmission line galloping," MDPI, 01. 2018.

[11] L. Manufacturing, "Real time transmission line conductor monitor," Publication number 11F-001 TLM, 08 2014.

[12] Overhead td solutions. USi. [Online]. Available: http://www.usi-power.com/power-donut-line-monitor/

[13] Transmission line conductor monitor. Lindsey. [Online]. Available: https://lindsey-usa.com/sensors/transmission-line-monitor/

[14] Secure cat-1 line monitoring. Nexans. [Online]. Available: https://www.nexans.no/eservice/Norway-no_NO/navigate_319184/Secure_Cat_1_line_monitoring.html

[15] Cat-1 transmission line monitoring system. Nexans. [Online]. Available: https://www.nexans.co.uk/eservice/UK-en_GB/navigate_191695/CAT_1_Transmission_Line_Monitoring_System.html

[16] Nexans, "Transmission line monitoring systems," Valley Group Brochure CAT-1, 06. 2009.

[17] Dlr monitoring sensor for distribution grids. Ampacimon. [Online]. Available: http://www.ampacimon.com/adr-sense-d/

[18] E. C. J.-L. LILIEN, "Uprating transmission lines through the use of an innovative real-time monitoring system," 2011 IEEE PES 12th International Conference on Transmission and Distribution Construction, Operation and Live-Line Maintenance (ESMO), 05. 2011.

[19] Span sentry dynamic line rating system. EDM. [Online]. Available: https://edmlink.com/products-edm/item/span-sentry-5

[20] Otlm sensor. Knill Group. [Online]. Available: https://www.otlm.eu/energy/otlm-device/

[21] Nytt medlem i smartgridsenteret – heimdall power. The norwegian Smart grid center. [Online]. Available: https://smartgrids.no/nytt-medlem-i-smartgridsenteret-heimdall-power/

[22] Heimdall power, the power of knowing. Heimdall Power. [Online]. Available: https://heimdallpower.com/

[23] "Ieee standard for calculating the current-temperature relationship of bare overhead conductors," *IEEE Std 738-2012 (Revision of IEEE Std 738-2006 - Incorporates IEEE Std 738-2012 Cor 1-2013)*, pp. 1–72, 2013.

[24] W. G. B2.43, "Guide for thermal rating calculations of overhead lines," TB-601, 2014.

[25] "Joule heating effect," Electromagnetics, 10 2014.

[26] L.Staszewski and W.Rebizant, "The differences between ieee and cigre heat balance concepts for line ampacity considerations," Wroclaw University of Technology, 09 2010.

[27] J.P.Holtzhausen, P.J.Pieterse, and H.J.Vermeulen, "Investigation of the effect of conductor temperature on ac power line corona," Department Electrical Engineering, Stellenbosch University, Stellenbosch, South Africa, 11 2010.

[28] C. W. G. B2.43, "Guide for thermal rating calculations of overhead lines," TB-601, 2014.

[29] M. Maksić, V. Djurica, A. Souvent, R. Trobec, and G. Kosec, "Dynamic thermal rating of power lines in raining conditions - model and measurements," 2016, pp. 1–5.

[30] H. A. Wheeler, "Formulas for the skin effect," *Proceedings of the IRE*, vol. 30, no. 9, pp. 412–424, 1942.

[31] J. Harrison, "Fast and accurate bessel function computation," in *2009 19th IEEE Symposium on Computer Arithmetic*, 2009, pp. 104–113.

[32] M. Lee, Y. Lee, and Y. Zohar, "The nusselt number in single-phase liquid flow forced convection in microchannels," in *2007 2nd IEEE International Conference on Nano/Micro Engineered and Molecular Systems*, 2007, pp. 502–506.

[33] Acsr 636 kcmil grosbeak (26/7). Nexans. [Online]. Available: https://www.nexans.pe/eservice/Peru-en/navigateproduct_540300242/ACSR_636_kcmil_GROSBEAK_26_7_.html

Appendices

APPENDIX A

Appendix - Monitor devices

A.1 DTLR monitoring methods

Monitor	Cost				Accuracy				
	Purchase cost	Install Cost	Maintain Cost	Line Outage	Measurement Reach	Normal Wind High Load	Normal Wind Low Load	Low Wind High Load	High Wind High Load
Weather	low	low	low	no	variable	good	good	low	good
Temperature	high	medium	high	no	variable	good	low	good	good
Tension	high	high	high	yes	multi-span	good	low	high	good
Sag	high	medium	high	no	variable	good	low	high	good
Clearance	high	medium	high	no	variable	good	low	high	good

Figure A.1: Monitoring methods for DTLR [2]

APPENDIX B

Appendix - Calculation of parameters

B.1 Magnetic core heating

Magnetic induction is found from

$$B_{max} = \mu_r \cdot \mu_0 \cdot H_{max} \tag{B.1}$$

where μ_r is the relative permeability of the steel wire, $\mu_0 = 4\pi \cdot 10^{-7}$ and H_{max} is given by

$$H_{max} = \sum_{n=1}^{p} (-1)^{n+1} \frac{In, max}{l_n} \tag{B.2}$$

where p is the total amount of non-ferrous layers, n is the number of the layers, I_{max} is the max value of the current in layer n, and l_n is the length of the wire in each layer [24].

B.2 Magnetic heating due to redistribution

The self inductive reactance of the layer of aluminum wires, due to longitudinal flux is given by

$$X_{nn} = 2\pi f \cdot \mu_0 \cdot \frac{(\frac{\pi}{4} \cdot D_n^2 - A_s) + \mu_r \cdot A_s}{l_n^2} \tag{B.3}$$

where $\mu_0 = 4\pi \cdot 10^{-7}$, μ_r is relative permeabilty of the core, A_s is the cross-sectional area of the core, l_n is the lay length of the layer, D_n is the mean diameter, and f is the frequency.

The mutual inductive reactance is given by

$$X_{pq} = X_{qp} = 2\pi f \cdot \mu_0 \cdot \frac{(\frac{\pi}{4} \cdot D_n^2 - A_s) + \mu_r \cdot A_s}{l_p \cdot l_q} \tag{B.4}$$

The increse in resistance is given by

$$R_{ac} = R_{dc} \cdot \frac{|Z_{tot}|}{R_{s1}} \tag{B.5}$$

where R_{s1}, the dc resistance of steel core and aluminium layer 1 or 3, is given by

$$R_{s1} = \frac{R_s \cdot R_1}{R_s + R_1} \tag{B.6}$$

and, the total impedance of one-layer conductor is given by

$$Z_{tot} = \frac{(Z_{ss} + Z_{s1}) \cdot (Z_{11} + Z_{s1})}{(Z_{ss} + 2 \cdot Z_{s1} + Z_{11})} \tag{B.7}$$

where Z_{ss} is the self impedance of steel core, Z_{s1} is the mutual impedance of steel core and aluminium layer, and Z_{11} is the self impedance of aluminium layer.

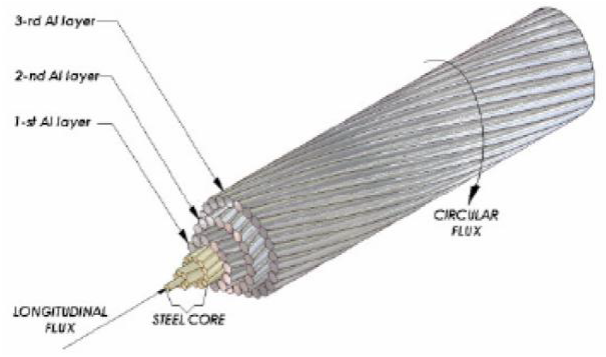

Figure B.1: Flux in non-ferrous layers in a steel core conductor [24]

B.3 Solar heating

The radiation on the surface of a conductor normal to the sun beam a height y above sea level can be written as

$$I_{B(y)} = I_{B(0)} \cdot [1 + 1.4 \cdot 10^{-4} \cdot y \cdot (\frac{1367}{I_{B(0)}} - 1)] \tag{B.8}$$

where H_S, the solar altitude can be expressed by the latitude, φ, and the declination, δ_S.

$$H_S = \arcsin(\sin(\varphi) \cdot \sin(\delta_S) + \cos(\varphi) \cdot \cos(\delta_S) \cdot \cos(Z)) \tag{B.9}$$

where Z is the hour angle of the sun. It increases with an angle of 15 degrees for every hour, $= 15 \cdot (12 - time)$.

B.4 Nusselt factor calculations

B.4.1 Forced convection

For forced convection and perpendicular air flow it has been shown that it is a correlasion between the Reynolds number, Re, and the the Nusselt number used when calculating convective cooling. One of the equations developed, that are based on several experiments is

$$Nu_{90} = B \cdot Re^n \tag{B.10}$$

where B and n is variables from table B.2. R_s in the table is the roughness of the conductor surface. For air flows that is not perpendicular adjustments

Smooth Conductors			Stranded Conductors, $R_s \leq 0.05$			Stranded Conductors, $R_s > 0.05$		
Re	***B***	***n***	***Re***	***B***	***n***	***Re***	***B***	***n***
35 - 5,000	0.583	0.471	100 - 2,650	0.641	0.471	100 - 2,650	0.641	0.471
5,000 - 50,000	0.148	0.633	2,650 - 50,000	0.178	0.633	2,650 - 50,000	0.048	0.800
50,000 - 200,000	0.0208	0.814						

Figure B.2: Table of coefficients for calculating convective cooling [24]

has to be done.

For smooth conductors

$$\frac{Nu_\delta}{Nu_{90}} = (\sin^2(\delta) + 0.0169 \cdot \cos^2(\delta))^{0.225} \tag{B.11}$$

For stranded conductor with $\delta \leq 24°$

$$\frac{Nu_\delta}{Nu_{90}} = 0.42 + 0.68 \cdot (\sin(\delta))^{1.08} \tag{B.12}$$

For stranded conductor with $\delta > 24°$

$$\frac{Nu_\delta}{Nu_{90}} = 0.43 + 0.58 \cdot (\sin(\delta))^{0.90} \tag{B.13}$$

This is valid for $Re < 4000$

B.4.2 Natural convection

When the wind is absent experiments have shown that there is a correlation between the Nusselt number and the Grashof and Prandtl numbers.

$$Nu_{nat} = A \cdot (Gr \cdot Pr)^m \tag{B.14}$$

the values for Pr, Gr, A and m can be found in table B.3. For inclination of

Range of $Gr \cdot Pr$		A	m
from	to		
10^{-1}	10^2	1.02	0.148
10^2	10^4	0.850	0.188
10^4	10^7	0.480	0.250
10^7	10^{12}	0.125	0.333

Figure B.3: Table of coefficients for calculating natural convective cooling [24]

a conductor towards the horizontal plane, β, the natural convective cooling is reduced by

$$\frac{Nu_\beta}{Nu_0} = 1 - 1.58 \cdot 10^{-4} \cdot \beta^{1.5} \tag{B.15}$$

for smooth conductor $\beta < 60°$, and

$$\frac{Nu_\beta}{Nu_0} = 1 - 1.76 \cdot 10^{-6} \cdot \beta^{2.5} \tag{B.16}$$

for stranded conductors, $\beta < 80°$

APPENDIX C

Matlab

C.1 Chnage in wind

```
clear all
I = 1000;                                   %current [A]

T_S = 40;                                   %temperature of conductor surface [C]
T_c = T_S+2;                                %core temperature of conductor [C]
T_av = (T_c + T_S)/2;                       %conductor mean temp [C]
T_a = 10;                                   %ambient temperature [C]

N_s = 0;                                    %clearness ratio []
N = 1;                                      %day of year
```

```
time = 1;                                          %time of day


for P = 1:10                                       %Precipitaion rate [mm*h^-1]
for u = 1:20                                       %wind speed [m/s]
%%%%%%%%%%%%%%%%%%%%%%%%%%%%%%%%%%%%%%%%%%%%%%%%%%%%%%%%%%%%%%%%%%%%%%%%%%
%Joule heating
k_sk = 1.08;                                       %skin effect factor between 1.02 - 1.08
D = 0.02;                                          %Outer diameter [m]

rho_0 = 2.65 * 10^(-8);                            %resistivty of alu, at 20 c [ohm * m]
alpha = 0.0042;                                    %tempreature coefficiant linear[1/K]
T_0 = 20;                                          %reference temperature [C]
zeta = 8*10^(-7);                                  %tempreature coefficiant quadratic[1/K^2]
%rho  = rho_0*(1 + alpha*(T_av-T_0)); %resistivty , linear
rho = rho_0*(1 + alpha *(T_av-T_0) + zeta *(T_av - T_0)^2);%resistivty , linear

z = [1 2 3 4];                                     % strand number
d_z = 0.0026;                                      %diameter of each wire
D_z = [0.0199 0.0147 0.0095 0.003];                %mean diameter of layer z
l_z = 1;                                           %lay lenght of layer z [m]
```

```
K_z = [sqrt(1 + (pi*D_z(1)/l_z)^2) sqrt(1 + (pi*D_z(2)/l_z)^2) sqrt(1 + (pi*D_z(3)/l_z)^2) sqrt(1 + (pi*D_z(4)/l_z)^2)];
R_dc20 = 1.404/1000;                                 %DC resistance 20 deg. [ohms/km] Per unit lenght!

R_dc_1 = 1/((((pi*d_z^2)/(4*rho))*(1 + (6*z(1)/K_z(1))+(6*z(2)/K_z(2))+(6*z(3)/K_z(3))+(6*z(4)/K_z(4))));  %DC resistance [ohm]
R_dc = R_dc20 * (1 + alpha*(T_av-20));        %DC resistance

%Joule heating
%q_j(u) = (4/(pi*D^2))*I^2 * R_dc; % [W/m^3]

q_j(u) = k_sk*I^2 * R_dc;

%uncertainties - calculation of R_dc
%%%%%%%%%%%%%%%%%%%%%%%%%%%%%%%%%%%%%%%%%%%%%%%%%%%%%%%%%%%%%%%%%%%%%%%%%%%%%%%%

%Solar heating
alpha_s = 0.5;                                       %absorbtivty of the surface of the conductor (0.2 new conductor, 0.9 old conductor)
radians = pi/180;

y = 10;                                              %height above sea level [m]
phi = 63*radians;                                    %latitude of conductor [rad]

F = 0.2;                                             %incident radiation reflected from ground, albedo []
Z = 15*(12-time)*radians;                            %hour angle of the sun [rad]
delta_s = 23.3*sin(2*pi*(284+N)/365)*radians;%declination [rad]
```

```
H_s = asin(sin(phi)*sin(delta_s)+cos(phi)*cos(delta_s)*cos(Z)); %solar altitude []
gamma_c = 3.34*radians;                          %Azimuth of conductor [rad]
gamma_s = asin(cos(delta_s)*sin(Z)/cos(H_s)); %Azimuth of the sun [rad]
eta = acos(cos(H_s)*cos(gamma_s-gamma_c));  %Angle of the solar beam with respect to axis of conductor[]
I_B0 = N_s * (1280*sin(H_s)/(sin(H_s)+0.314));%Solar radiation on surface normal to the sun at sea level [W/m^2]
I_B = I_B0 * (1 + 1.14*10^(-4)*y*((1367/I_B0)-1)); %Solar radiation on surface normal to the sun [W/m^2]
I_d = (430.5-0.3288*I_B)*sin(H_s); %diffuse sky radiation to a horizontal surface [W/m^2]
I_T = I_B*(sin(eta) + pi *F * sin(H_s)/2)+ I_d*(1 + pi*F/2); %solar intensity [W/m]

q_s(u) = (alpha_s*I_T*D);                               %[W/m^2]

%uncertainties -
% %%%%%%%%%%%%%%%%%%%%%%%%%%%%%%%%%%%%%%%%%%%%%%%%%%%%%%%%%%%%%%%%%%
%Heat distribution
lambda = 36.9;                                   %conductvity of aluminium [Siemens/m]

T_c = (q_j(u))/(4*pi*lambda)+T_S;           %conductor core temperature   [C]
T_av = (T_c + T_S)/2;                             %conductor mean temp [C]

%uncertainties -
% %%%%%%%%%%%%%%%%%%%%%%%%%%%%%%%%%%%%%%%%%%%%%%%%%%%%%%%%%%%%%%%%%%
%Convective cooling
```

```
77 rho_a = 1.225;                                    %density of
       air[kg/m^3]
78 mu = 1.81*10^(-5);                                %viscosity
      of air[kg/m*s]
79 delta= 5*radians;                                 %angle wind
       vs conductor [rad]
80 beta = 5*radians;                                 %
      inclination of conductor towards horizontal plane[
      rad]
81 gamma_c = 3.34*radians;                           %azimuth of
       conductor[rad]
82 %Nusselt
83 B = 0.178; %found in table b2
84 n = 0.633; %found in table b2
85 A = 0; %found in table B3
86 Gr = 0; %found in table B3
87 Pr = 0; %found in table B3
88 m = 0; %found in table B3
89 Nu_i = 12; % 11 = forced conv smooth cond, 12=forced
      conve strand cond, 21 = natural conv smooth cond,
      22=natural conve strand con
90 Re = (rho_a*D*u)/mu; %Reynholds number
91 Nu_90 = B*Re^n;
92 Nu_beta = A *(Gr * Pr)^m;
93 if Nu_i == 11
94     Nu = Nu_90*(sin(delta)^2 + 0.0169*cos(delta)^2)
          ^0.225;
95 elseif Nu_i==12
96      if delta<=24
97          Nu = Nu_90*(0.42+0.68*(sin(delta))^1.08);
98      else
99          Nu = Nu_90*(0.43+0.58*(sin(delta))^0.9);
100     end
101 elseif Nu_i==21
102     Nu = Nu_beta*(1-1.58*10^(-4)*beta^(1.5));
103 elseif Nu_i==22
104     Nu = Nu_beta*(1-1.76*10^(-6)*beta^(2.5));
105 end
```

```

T_f = (T_a+T_S)/2;                                    %film temperature [C]
lambda_a = 2.368*10^(-2) + 7.23*10^(-5)*(T_f+273) - 2.763*10^(-8)*(T_f+273)^2; %air thermal conductivity [W/mK]
h_a = Nu*lambda_a/D;                                  %convection coeffeficiant

%Convective cooling
q_c(u) = -h_a*(T_S-T_a); %[W/m^2]

%uncertainties - regarding nusselt ,NU or h.
%%%%%%%%%%%%%%%%%%%%%%%%%%%%%%%%%%%%%%%%%%%%%%%%%%%%%%%%%%%%%%%%%%%%%%%%%%%%%%%%
%radiative cooling

sigma_B = 5.6697*10^(-7);                             %Stefan Boltzmann constant [WM^-2K^-4]
epsilon_s = 0.4;                                      %Emissivity of the surface of the conductor

%radiative cooling
q_r(u) = - sigma_B * epsilon_s * ((T_S+273)^4-(T_a+273)^4); %[W/m^2]

%uncertainties - high value??
%%%%%%%%%%%%%%%%%%%%%%%%%%%%%%%%%%%%%%%%%%%%%%%%%%%%%%%%%%%%%%%%%%%%%%%%%%%%%%%%
%impinged cooling
c_w = 4200;                                           %Specific heat of water [J/kg*C]

rho_w = 997;                                          %water density [kg/m^3]
```

```
f_p = sqrt((P*rho_w*10^(-3)/3600)^2 + (u*6.71^(-5)*P^(0.84))^2); %rain mass flux

%impinged cooling
q_im(u) = -(0.71/pi) * c_w * f_p *(T_S - T_a); % [W/m^2]

lambda_w = 0.014;
h_w = Nu*lambda_w/D;                                %convection water
%%%%%%%%%%%%%%%%%%%%%%%%%%%%%%%%%%%%%%%%%%%%%%%%%%%%%%%%%%%%%%%%%%%%%%%%
%evaporative cooling
L_e = 2260;                                         %evaporative Laten heat of water [kJ/kg]
C_p = 1;                                            %Specific heat of air [kJ/kg]
k = 0.62;                                           %Rate of molecular weights of water vapour and dry air
p = 1013.25;                                        %air pressure [hPa]

R_v = 0.461;                                        %[kJ/kgK]
e_s0 = 6.1;                                         %saturation presure reference [hPa]
e_s = e_s0 * exp((L_e/R_v)*(1/(273)-1/(T_c+273))); %Saturation presure [hPa]
W_f = (atan(1600*f_p))/((pi/2)+ 1.6);               %Wetted factor []
f_e = h_w*k/C_p *(1-D/2)*e_s/p;                     %evaporation mass flux[kg/m^2*s]

%q_e(u) = 0.5 * q_im(u) * (k*L_e/C_p)*((1-D/2)*e_s/p);

q_e(u) = - W_f*f_e*L_e; %[W/m^2]

%uncertainties - r=radii?? - [hPa] or [Pa]
```

```
%
    %%%%%%%%%%%%%%%%%%%%%%%%%%%%%%%%%%%%%%%%%%%%%%%%%%%%%%%%%%%%%%%%%%%%%%%%%%%%%

q_1(u)=q_j(u) + q_c(u) + q_r(u) + q_im(u) + q_e(u);
q_2(u)=q_j(u) + q_c(u) + q_r(u);
end

u=1:20;

hold on

%
figure(1);
if P == 1
xlabel('Wind speed [m/s]');
ylabel('Heating of conductor [W/m]');
axis([1 20 -3500 2000]);
grid on
plot(u,q_e);
plot(u,q_im);

plot(u,q_j);
plot(u,q_r);
plot(u,q_c);
legend({'q_e','q_i','q_j','q_r','q_c'},'Location','best
    ')
end
%}
%
figure (2);
xlabel('Wind speed [m/s]');
ylabel('Heating of conductor [W/m]');
axis([1 20 -4500 500]);
grid on
plot(u,q_1,'b');
plot(u,q_2,'r');
%}
```

```
end
legend({'q_1','q_2'},'Location','best');
```

C.2 Chnage in ambient temperature

```
clear all
I = 1000;                                    %current [A]

T_S = 40;                                    %temperature of conductor surface  [C]
T_c = T_S+2;                                 %core temperature of conductor [C]
T_av = (T_c + T_S)/2;                        %conductor mean temp [C]

N_s = 0;                                     %clearness ratio []
N = 1;                                       %day of year
time = 1;                                    %time of day

u = 1;                                       %wind speed [m/s]

for P = 1:10                                 %Precipitaion rate [mm*h^-1]
for T_a = 1:30                               %ambient temperature  [C]
%%%%%%%%%%%%%%%%%%%%%%%%%%%%%%%%%%%%%%%%%%%%%%%%%%%%%%%%%%%%%%%%%%%%%%%%%%%
%Joule heating
k_sk = 1.08;                                 %skin effect factor  between 1.02 - 1.08
D = 0.02;                                    %Outer diameter [m]
```

```
20
21 rho_0 = 2.65 * 10^(-8);                          %resistivty
       of alu, at 20 c [ohm * m]
22 alpha = 0.0042;                                  %
   tempreature coefficiant linear[1/K]
23 T_0 = 20;                                        %reference
   temperature [C]
24 zeta = 8*10^(-7);                                %
   tempreature coefficiant quadratic[1/K^2]
25 %rho  = rho_0*(1 + alpha*(T_av-T_0)); %resistivty,
   linear
26 rho = rho_0*(1 + alpha *(T_av-T_0) + zeta *(T_av - T_0)
   ^2);%resistivty, linear
27
28 z = [1 2 3 4];                                    % strand
   number
29 d_z = 0.0026;                                    %diameter
   of each wire
30 D_z = [0.0199 0.0147 0.0095 0.003];              %mean
   diameter of layer z
31 l_z = 1;                                         %lay lenght
       of layer z [m]
32 K_z = [sqrt(1 + (pi*D_z(1)/l_z)^2) sqrt(1 + (pi*D_z(2)/
   l_z)^2) sqrt(1 + (pi*D_z(3)/l_z)^2) sqrt(1 + (pi*D_z
   (4)/l_z)^2)];
33 R_dc20 = 1.404/1000;                             %DC
   resistance 20 deg. [ohms/km] Per unit lenght!
34
35 %R_dc = 1/(((pi*d_z^2)/(4*rho))*(1 + (6*z(1)/K_z(1))
   +(6*z(2)/K_z(2))+(6*z(3)/K_z(3))+(6*z(4)/K_z(4))));
   %DC resistance [ohm]
36 R_dc = R_dc20 * (1 + alpha*(T_av-20));            %DC
   resistance
37
38 %Joule heating
39 %q_j(u) = (4/(pi*D^2))*I^2 * R_dc; % [W/m^3]
40
41 q_j(T_a) = k_sk*I^2 * R_dc;
```

```
%uncertainties - calculation of R_dc
% %%%%%%%%%%%%%%%%%%%%%%%%%%%%%%%%%%%%%%%%%%%%%%%%%%%%%%%%%%%%%%%%%%%%%%%%%%%%%%
%Solar heating
alpha_s = 0.5;                              % absorbtivty of the surface of the conductor (0.2 new conductor, 0.9 old conductor)
radians = pi/180;

y = 10;                                     %height above sea level [m]
phi = 63*radians;                           %latitude of conductor [rad]

F = 0.2;                                    %incident radiation reflected from ground, albedo []
Z = 15*(12-time)*radians;                   %hour angle of the sun [rad]
delta_s = 23.3*sin(2*pi*(284+N)/365)*radians;% declination [rad]
H_s = asin(sin(phi)*sin(delta_s)+cos(phi)*cos(delta_s)*cos(Z)); %solar altitude []
gamma_c = 3.34*radians;                     %Azimuth of conductor [rad]
gamma_s = asin(cos(delta_s)*sin(Z)/cos(H_s)); %Azimuth of the sun [rad]
eta = acos(cos(H_s)*cos(gamma_s-gamma_c));  %Angle of the solar beam with respect to axis of conductor[]
I_B0 = N_s * (1280*sin(H_s)/(sin(H_s)+0.314));%Solar radiation on surface normal to the sun at sea level [W/m^2]
I_B = I_B0 * (1 + 1.14*10^(-4)*y*((1367/I_B0)-1)); % Solar radiation on surface normal to the sun [W/m^2]
I_d = (430.5-0.3288*I_B)*sin(H_s); %diffuse sky radiation to a horizontal surface [W/m^2]
I_T = I_B*(sin(eta) + pi *F * sin(H_s)/2)+ I_d*(1 + pi*
```

```
    F/2); %solar intensity [W/m]

q_s = (alpha_s*I_T*D);                                  %[W/m^2]

%uncertainties -
% %%%%%%%%%%%%%%%%%%%%%%%%%%%%%%%%%%%%%%%%%%%%%%%%%%%%%%%%%%%%%%%%%%%%%%%%%%%%%%%%
%Heat distribution
lambda = 36.9;                                          % conductvity of aluminium [Siemens/m]

T_c = (q_j(T_a))/(4*pi*lambda)+T_S;                     %conductor core temperature [C]
T_av = (T_c + T_S)/2;                                   %conductor mean temp [C]

%uncertainties -
% %%%%%%%%%%%%%%%%%%%%%%%%%%%%%%%%%%%%%%%%%%%%%%%%%%%%%%%%%%%%%%%%%%%%%%%%%%%%%%%%
%Convective cooling
rho_a = 1.225;                                          %density of air[kg/m^3]
mu = 1.81*10^(-5);                                      %viscosity of air[kg/m*s]
delta= 5*radians;                                       %angle wind vs conductor [rad]
beta = 5*radians;                                       % inclination of conductor towards horizontal plane[rad]
gamma_c = 3.34*radians;                                 %azimuth of conductor[rad]
%Nusselt
B = 0.178; %found in table b2
n = 0.633; %found in table b2
A = 0; %found in table B3
Gr = 0; %found in table B3
```

```
Pr = 0; %found in table B3
m = 0; %found in table B3
Nu_i = 12; % 11 = forced conv smooth cond, 12=forced
    conve strand cond, 21 = natural conv smooth cond,
    22=natural conve strand con
Re = (rho_a*D*u)/mu; %Reynholds number
Nu_90 = B*Re^n;
Nu_beta = A *(Gr * Pr)^m;
if Nu_i == 11
    Nu = Nu_90*(sin(delta)^2 + 0.0169*cos(delta)^2)
        ^0.225;
elseif Nu_i==12
     if delta<=24
         Nu = Nu_90*(0.42+0.68*(sin(delta))^1.08);
     else
         Nu = Nu_90*(0.43+0.58*(sin(delta))^0.9);
     end
elseif Nu_i==21
     Nu = Nu_beta*(1-1.58*10^(-4)*beta^(1.5));
elseif Nu_i==22
     Nu = Nu_beta*(1-1.76*10^(-6)*beta^(2.5));
end

T_f = (T_a+T_S)/2;                                  %film
    temperature [C]
lambda_a = 2.368*10^(-2) + 7.23*10^(-5)*(T_f+273) -
    2.763*10^(-8)*(T_f+273)^2; %air thermal conductivity
     [W/mK]
h_a = Nu*lambda_a/D;                                %
    convection coeffeficiant

%Convective cooling
q_c(T_a) = -h_a*(T_S-T_a); %[W/m^2]

%uncertainties - regarding nusselt,NU or h.
%
    %%%%%%%%%%%%%%%%%%%%%%%%%%%%%%%%%%%%%%%%%%%%%%%%%%%%%%%%%%%%%%%%%%%%%%%%%%%%%%%%
```

```
%radiative cooling

sigma_B = 5.6697*10^(-7);                   %Stefan Boltzmann constant [WM^-2K^-4]
epsilon_s = 0.4;                            %Emissivity of the surface of the conductor

%radiative cooling
q_r(T_a) = - sigma_B * epsilon_s * ((T_S+273)^4-(T_a+273)^4); %[W/m^2]

%uncertainties - high value??
%%%%%%%%%%%%%%%%%%%%%%%%%%%%%%%%%%%%%%%%%%%%%%%%%%%%%%%%%%%%%%%%%%%%%%%%%%%%

%impinged cooling
c_w = 4200;                                 %Specific heat of water [J/kg*C]

rho_w = 997;                                %water density [kg/m^3]
f_p = sqrt((P*rho_w*10^(-3)/3600)^2 + (u*6.71^(-5)*P^(0.84))^2); %rain mass flux

%impinged cooling
q_im(T_a) = -(0.71/pi) * c_w * f_p *(T_S - T_a); % [W/m^2]

lambda_w = 0.014;
h_w = Nu*lambda_w/D;                        %convection water
%%%%%%%%%%%%%%%%%%%%%%%%%%%%%%%%%%%%%%%%%%%%%%%%%%%%%%%%%%%%%%%%%%%%%%%%%%%%

%evaporative cooling
L_e = 2260;                                 %evaporative Laten heat of water [kJ/kg]
C_p = 1;                                    %Specific
```

```
    heat of air [kJ/kg]
k = 0.62;                                        %Rate of
    molecular weights of water vapour and dry air
p = 1013.25;                                     %air
    pressure [hPa]

R_v = 0.461;                                     %[kJ/kgK]
e_s0 = 6.1;                                      %saturation
     presure reference [hPa]
e_s = e_s0 * exp((L_e/R_v)*(1/(273)-1/(T_c+273))); %
    Saturation presure [hPa]
W_f = (atan(1600*f_p))/((pi/2)+ 1.6);            %Wetted
    factor []
f_e = h_w*k/C_p *(1-D/2)*e_s/p;                  %
    evaporation mass flux[kg/m^2*s]

%q_e(u) = 0.5 * q_im(u) * (k*L_e/C_p)*((1-D/2)*e_s/p);

q_e(T_a) = - W_f*f_e*L_e; %[W/m^2]

%uncertainties - r=radii?? - [hPa] or [Pa]
%
    %%%%%%%%%%%%%%%%%%%%%%%%%%%%%%%%%%%%%%%%%%%%%%%%%%%%%%%%%%%%%%%%%%%%%%%%%%%%%%%%%%%%%%


q_1(T_a)=q_j(T_a) + q_c(T_a) + q_r(T_a) + q_im(T_a) +
    q_e(T_a);
q_2(T_a)=q_j(T_a) + q_c(T_a) + q_r(T_a);
end

T_a = 1:30;

hold on

%
if P == 1
figure (1)
xlabel('Ambient temperature [C]');
```

```
169 ylabel('Heating of conductor [W/m]');
170 axis([10 30 -1000 2000]);
171 grid on
172 plot(T_a,q_e);
173 plot(T_a,q_im);
174
175 plot(T_a,q_j);
176 plot(T_a,q_r);
177 plot(T_a,q_c);
178 legend({'q_e','q_i','q_j','q_r','q_c'},'Location','best
    ')
179 end
180 %}
181 %
182 figure (2);
183 xlabel('Ambient temperature [C]');
184 ylabel('Heating of conductor [W/m]');
185 axis([1 30 -250 1500]);
186 grid on
187 plot(T_a,q_1,'b');
188 plot(T_a,q_2,'r');
189 %}
190
191 end
192 legend({'q_1','q_2'},'Location','best');
```

C.3 Chnage in conductor temperature

```
1 clear all
2 I = 1000;                                    %current [A
    ]
3                                   %temperature of
                                       conductor surface  [
                                       C]
4 T_c = T_S+2;                                 %core
    temperature of conductor [C]
5 T_av = (T_c + T_S)/2;                        %conductor
    mean temp [C]
```

```
T_a = 10;                                        %ambient temperature   [C]

N_s = 0;                                         %clearness ratio  []
N = 1;                                           %day of year
time = 1;                                        %time of day

u = 1;                                           %wind speed  [m/s]

for P = 1:10                                     %Precipitaion rate [mm*h^-1]
for T_S = 1:80                                   %Surface temperature [C]
%%%%%%%%%%%%%%%%%%%%%%%%%%%%%%%%%%%%%%%%%%%%%%%%%%%%%%%%%%%%%%%%%%%%%%%%
%Joule heating
k_sk = 1.08;                                     %skin effect factor  between 1.02 - 1.08
D = 0.02;                                        %Outer diameter [m]

rho_0 = 2.65 * 10^(-8);                          %resistivty  of alu, at 20 c [ohm * m]
alpha = 0.0042;                                  %tempreature coefficiant linear[1/K]
T_0 = 20;                                        %reference temperature [C]
zeta = 8*10^(-7);                                %tempreature coefficiant quadratic[1/K^2]
%rho  = rho_0*(1 + alpha*(T_av-T_0)); %resistivty, linear
rho = rho_0*(1 + alpha *(T_av-T_0) + zeta *(T_av - T_0)^2);%resistivty, linear
```

```
z = [1 2 3 4];                                  % strand number
d_z = 0.0026;                                   %diameter of each wire
D_z = [0.0199 0.0147 0.0095 0.003];             %mean diameter of layer z
l_z = 1;                                        %lay lenght of layer z [m]
K_z = [sqrt(1 + (pi*D_z(1)/l_z)^2) sqrt(1 + (pi*D_z(2)/l_z)^2) sqrt(1 + (pi*D_z(3)/l_z)^2) sqrt(1 + (pi*D_z(4)/l_z)^2)];
R_dc20 = 1.404/1000;                            %DC resistance 20 deg. [ohms/km] Per unit lenght!

%R_dc = 1/(((pi*d_z^2)/(4*rho))*(1 + (6*z(1)/K_z(1))+(6*z(2)/K_z(2))+(6*z(3)/K_z(3))+(6*z(4)/K_z(4)))); %DC resistance [ohm]
R_dc = R_dc20 * (1 + alpha*(T_av-20));          %DC resistance

%Joule heating
%q_j(T_S) = (4/(pi*D^2))*I^2 * R_dc; % [W/m^3]

q_j(T_S) = k_sk*I^2 * R_dc;

%uncertainties - calculation of R_dc
%%%%%%%%%%%%%%%%%%%%%%%%%%%%%%%%%%%%%%%%%%%%%%%%%%%%%%%%%%%%%%%%%%%%%%%%%%%%%%%%%%%%

%Solar heating
alpha_s = 0.5;                                  %absorbtivty of the surface of the conductor (0.2 new conductor, 0.9 old conductor)
radians = pi/180;

y = 10;                                         %height above sea level [m]
```

```
phi = 63*radians;                         %latitude of conductor [rad]

F = 0.2;                                  %incident radiation reflected from ground, albedo []
Z = 15*(12-time)*radians;                 %hour angle of the sun [rad]
delta_s = 23.3*sin(2*pi*(284+N)/365)*radians;% declination [rad]
H_s = asin(sin(phi)*sin(delta_s)+cos(phi)*cos(delta_s)*cos(Z)); %solar altitude []
gamma_c = 3.34*radians;                   %Azimuth of conductor [rad]
gamma_s = asin(cos(delta_s)*sin(Z)/cos(H_s)); %Azimuth of the sun [rad]
eta = acos(cos(H_s)*cos(gamma_s-gamma_c)); %Angle of the solar beam with respect to axis of conductor[]
I_B0 = N_s * (1280*sin(H_s)/(sin(H_s)+0.314));%Solar radiation on surface normal to the sun at sea level [W/m^2]
I_B = I_B0 * (1 + 1.14*10^(-4)*y*((1367/I_B0)-1)); % Solar radiation on surface normal to the sun [W/m^2]
I_d = (430.5-0.3288*I_B)*sin(H_s); %diffuse sky radiation to a horizontal surface [W/m^2]
I_T = I_B*(sin(eta) + pi *F * sin(H_s)/2)+ I_d*(1 + pi*F/2); %solar intensity [W/m]

q_s(T_S) = (alpha_s*I_T*D);               %[W/m^2]

%uncertainties -
% %%%%%%%%%%%%%%%%%%%%%%%%%%%%%%%%%%%%%%%%%%%%%%%%%%%%%%%%%%%%%%%%%%%%%%%%%%%%%%%%%%%

%Heat distribution
lambda = 36.9;                            % conductvity of aluminium [Siemens/m]

```

```
T_c = (q_j(T_S))/(4*pi*lambda)+T_S;          %conductor core temperature   [C]
T_av = (T_c + T_S)/2;                        %conductor mean temp [C]

%uncertainties  -
% %%%%%%%%%%%%%%%%%%%%%%%%%%%%%%%%%%%%%%%%%%%%%%%%%%%%%%%%%%%%%%%%%%%%%%
%Convective cooling
rho_a = 1.225;                               %density of air[kg/m^3]
mu = 1.81*10^(-5);                           %viscosity of air[kg/m*s]
delta= 5*radians;                            %angle wind vs conductor [rad]
beta = 5*radians;                            %inclination of conductor towards horizontal plane[rad]
gamma_c = 3.34*radians;                      %azimuth of conductor[rad]
%Nusselt
B = 0.178; %found in table b2
n = 0.633; %found in table b2
A = 0; %found in table B3
Gr = 0; %found in table B3
Pr = 0; %found in table B3
m = 0; %found in table B3
Nu_i = 12; % 11 = forced conv smooth cond, 12=forced conve strand cond, 21 = natural conv smooth cond, 22=natural conve strand con
Re = (rho_a*D*u)/mu; %Reynholds number
Nu_90 = B*Re^n;
Nu_beta = A *(Gr * Pr)^m;
if Nu_i == 11
    Nu = Nu_90*(sin(delta)^2 + 0.0169*cos(delta)^2)^0.225;
elseif Nu_i==12
```

```
        if delta<=24
            Nu = Nu_90*(0.42+0.68*(sin(delta))^1.08);
        else
            Nu = Nu_90*(0.43+0.58*(sin(delta))^0.9);
        end
    elseif Nu_i==21
        Nu = Nu_beta*(1-1.58*10^(-4)*beta^(1.5));
    elseif Nu_i==22
        Nu = Nu_beta*(1-1.76*10^(-6)*beta^(2.5));
end

T_f = (T_a+T_S)/2;                                    %film temperature [C]
lambda_a = 2.368*10^(-2) + 7.23*10^(-5)*(T_f+273) - 2.763*10^(-8)*(T_f+273)^2; %air thermal conductivity [W/mK]
h_a = Nu*lambda_a/D;                                  % convection coeffeficiant

%Convective cooling
q_c(T_S) = -h_a*(T_S-T_a); %[W/m^2]

%uncertainties - regarding nusselt,NU or h.
% %%%%%%%%%%%%%%%%%%%%%%%%%%%%%%%%%%%%%%%%%%%%%%%%%%%%%%%%%%%%%%%%%%%%%%%%%%%%%%%%%%%%

%radiative cooling

sigma_B = 5.6697*10^(-7);                             %Stefan Boltzmann constant [WM^-2K^-4]
epsilon_s = 0.4;                                      %Emissivity of the surface of the conductor

%radiative cooling
q_r(T_S) = - sigma_B * epsilon_s * ((T_S+273)^4-(T_a+273)^4); %[W/m^2]

%uncertainties - high value??
```

```
%%%%%%%%%%%%%%%%%%%%%%%%%%%%%%%%%%%%%%%%%%%%%%%%%%%%%%%%%%%%%%%%%%%%%%%%%%
%impinged cooling
c_w = 4200;                                 %Specific heat of water [J/kg*C]

rho_w = 997;                                %water density [kg/m^3]
f_p = sqrt((P*rho_w*10^(-3)/3600)^2 + (u*6.71^(-5)*P^(0.84))^2); %rain mass flux

%impinged cooling
q_im(T_S) = -(0.71/pi) * c_w * f_p *(T_S - T_a); % [W/m^2]

lambda_w = 0.014;
h_w = Nu*lambda_w/D;                        %convection water
%%%%%%%%%%%%%%%%%%%%%%%%%%%%%%%%%%%%%%%%%%%%%%%%%%%%%%%%%%%%%%%%%%%%%%%%%%
%evaporative cooling
L_e = 2260;                                 %evaporative Laten heat of water [kJ/kg]
C_p = 1;                                    %Specific heat of air [kJ/kg]
k = 0.62;                                   %Rate of molecular weights of water vapour and dry air
p = 1013.25;                                %air pressure [hPa]

R_v = 0.461;                                %[kJ/kgK]
e_s0 = 6.1;                                 %saturation presure reference [hPa]
e_s = e_s0 * exp((L_e/R_v)*(1/(273)-1/(T_c+273))); % Saturation presure [hPa]
W_f = (atan(1600*f_p))/((pi/2)+ 1.6);      %Wetted
```

```
    factor []
f_e = h_w*k/C_p *(1-D/2)*e_s/p;                %
    evaporation mass flux[kg/m^2*s]

%q_e(u) = 0.5 * q_im(u) * (k*L_e/C_p)*((1-D/2)*e_s/p);

q_e(T_S) = - W_f*f_e*L_e; %[W/m^2]

%
    %%%%%%%%%%%%%%%%%%%%%%%%%%%%%%%%%%%%%%%%%%%%%%%%%%%%%%%%%%%%%%%%%%%%%%%%%%%%%%%%%%%%


q_1(T_S)=q_j(T_S) + q_c(T_S) + q_r(T_S) + q_im(T_S) +
    q_e(T_S);
q_2(T_S)=q_j(T_S) + q_c(T_S) + q_r(T_S);

end

T_S = 1:80;

hold on

%T-S
%
figure (1);
if P == 1
xlabel('Surface temperature of conductor [C]');
ylabel('Heating of conductor [W/m]');
axis([10 80 -2200 2500]);
grid on
plot(T_S,q_e);
plot(T_S,q_im);

plot(T_S,q_j);
plot(T_S,q_r);
plot(T_S,q_c);
legend({'q_e','q_i','q_j','q_r','q_c'},'Location','best
    ')
```

```
180 end
181 %}
182 %
183 figure (2);
184 xlabel('Surface temperature of conductor [C]');
185 ylabel('Heating of conductor [W/m]');
186 axis([10 80 -3000 1500]);
187 grid on
188 plot(T_S,q_1,'b');
189 plot(T_S,q_2,'r');
190 %}
191
192 end
193 legend({'q_1','q_2'},'Location','best');
```

NTNU

Norwegian University of
Science and Technology